Electronic Supplementary Material (ESI) for Sensors & Diagnostics.

Electronic Supplementary Information

for the manuscript entitled

A Zn-MOF functionalized with alkyne groups: Ultrasensitive detection of Cu^{+} and Pd^{2+} ions in aqueous medium

Aashish, Ruchika Gupta, Rajeev Gupta*

Department of Chemistry, University of Delhi, Delhi–110007

Experimental Section

Materials and methods

All chemicals and reagents were procured from the commercial companies and were used without further purification. The solvents were purified utilizing the standard literature methods.[1]

Physical measurements

The FTIR spectra were recorded using an Agilent Cary – 630 spectrometer having a diamond ATR. NMR spectral measurements were done with a Jeol 400 MHz spectrometer. UV Visible spectra were recorded using a PerkinElmer Lambda-950 spectrophotometer. Fluorescence spectral studies were performed with a Cary Eclipse fluorescence spectrometer. Time-resolved fluorescence spectra were recorded using a picosecond fluorimeter from Horiba Jobin Yvon (FluoroHub). Photoluminescence studies were performed using a QM-8450-11 Quanta master up-conversion and down-conversion fluorescence spectrometer, equipped with a 450W Xe source lamp. Elemental analysis was carried out using an Elementar Analysen Systeme GmbH Vario EL-III instrument. Powder X-ray diffraction (PXRD) patterns were obtained either with a Rigaku Table-Top XRD or a Bruker AXS D8 Discover instrument (Cu Kα radiation, λ = 1.54184 Å). The samples were ground and subjected to a range of θ = 5–60° at a slow scan rate at room temperature. Thermal gravimetric analysis (TGA) and differential scanning calorimetry (DSC) were performed with a Shimadzu DTG-60 and TA-DSC Q200 instruments, respectively, under a N_2 atmosphere with a heating rate of 10 °C per min. The nitrogen sorption isotherms were collected using a Quantachrome gas sorption analyzer. Barrett-Joyner-Halenda (BJH) model was used for the analysis of pore size based on N_2 adsorption. SEM and EDX measurements were performed with a Jeol SM 6610 LV instrument. ζ potentials were measured using a Malvern Zetasizer ZS90 instrument. For these studies, powdered samples were suspended in water followed by sonication to obtain a stable suspension. XPS studies were performed with a Kratos Analytical Axis Supra model.

X-ray diffraction studies

Single crystal X-ray diffraction data for Zn-MOFs **1** and **2** were collected on a Rigaku Oxford XtaLAB Synergy-DW diffractometer or a Bruker SMART APEX-II CCD diffractometer equipped with a graphite monochromatic MoKα radiation (λ = 0.71073 Å).[2] For **1**, SMART[3] was used for collecting frames of data, indexing reflections and determining the lattice parameters; SAINT[3] for integration of the intensity of reflections and scaling; and SADABS[4]

for absorption correction. The frames were collected at 293(2) K. The structures were solved by the direct methods using SIR-97[5] and refined by the full-matrix least-squares refinement techniques on F^2 using SHELXL-97[6] incorporated in Olex2 crystallographic package.[7] All calculations and structure refinements were performed using Olex2 programme. The hydrogen atoms were fixed at the calculated positions using the isotropic thermal parameters whereas non-hydrogen atoms were refined anisotropically. The hydrogen atoms of the coordinated as well as uncoordinated water molecules could not be located from the Fourier map; however, their contributions are included in the empirical formulae. The crystallographic data collection and structure solution parameters are presented in Tables S1 and S5 whereas selected bond distances and bond angles are presented in Tables S2 and S3; and Tables S6 and S7. CCDC Nos. 2282501 (**1**) and 2282500 (**2**) contain the supplementary crystallographic data for this paper.

Fluorescence spectral measurements

For sensing studies, 1 mg of MOF **1** was suspended in 4 mL of water, followed by 30 min of ultrasonication. Stock solutions of metal salts (2.5 mM; $HgCl_2$, $PtCl_2$, $Cu(OAc)_2$, $AgNO_3$, $Pb(OAc)_2$, $Co(OAc)_2$, $Zn(OAc)_2$, $Cd(OAc)_2$, $Mg(NO_3)_2$, $CrCl_3$, $NiCl_2$, $Mn(OAc)_2$, NaCl, KCl, $Al(NO_3)_3$, $FeCl_2$, CuCl, and $PdCl_2$ were prepared in H_2O. All fluorescence spectral experiments were performed with a 1.0 cm path length cuvette at 25±1 °C in H_2O.

Determination of Stern-Volmer (K_{SV}) and binding (K_b) constants

Stern-Volmer constants (K_{SV}) were calculated using the Stern-Volmer equation (1), where I_0 and I are the emission intensities of **1** in the absence and presence of a metal ion used as a quencher (Q), respectively.[8,9] The binding constants (K_b) were computed using the Benesi-Hildebrand equation (2),[10] where I is the emission intensity of **1** in the presence of $[Cu^+]$ or $[Pd^{2+}]$ ions at 435 nm, respectively; I_0 is the intensity of **1** in the absence of $[Cu^+]$ or $[Pd^{2+}]$ ions; and I_{min} is the minimum fluorescence intensity in the presence of $[Cu^+]$ or $[Pd^{2+}]$ ions. K_b was obtained by a ratio of intercept and slope in $1/(I\text{-}I_0)$ vs. 1/[M] plot, where M refers to a respective metal ion.

$$I_0/I = 1 + K_{SV}[M] \quad (1)$$

$$1/(I\text{-}I_0) = 1/\{K_b(I_0\ \ I_{min})[M]\} + 1/(\ I_0\ \ I_{min}) \quad (2)$$

Determination of detection limit

The detection limits were calculated using the equation (3), where *k* is the slope of a plot of fluorescence intensity of **1** at 435 nm vs. metal ion concentration and σ is the standard deviation of ten blank fluorescence measurements of **1**.[11]

Detection limit = $3\sigma/k$ (3)

Inclusion studies

30 mg sample of MOF **1** was suspended in MeCN and impregnated with 5 equiv. of Cu^{+} or Pd^{2+} ions for 12 h at 25 °C. The impregnated sample was filtered, washed thrice with fresh MeCN, and dried under vacuum. This sample was used for the characterization.

Calculation of overlap integral

The overlap integral between the emission spectrum of **1** and the absorption spectrum of Pd^{2+} ion was calculated using the equation (4).[12]

$$J(\lambda) = \int_0^\infty F_D(\lambda)\, \varepsilon_A(\lambda)\, \lambda^4 d\lambda \quad (4)$$

Herein, λ is wavelength, $F_D(\lambda)$ represents the normalized emission intensity of the donor 1 (normalized to unity) and $\varepsilon_A(\lambda)$ is the molar extinction coefficient of the acceptor (Pd^{2+} ion) in $mol^{-1}cm^{-1}$.

Fabrication of filter paper strips

Strips of Whatman filter paper were dipped in a suspension of **1** followed by drying in air to prepare the test strips. Such **1**-coated test strips were directly dipped into an aqueous solution of either Cu^{+} or Pd^{2+} ion. These test strips were then investigated under the UV light.

References

1. D. D. Perrin, W. L. F. Armarego, D. R. Perin, Purification of Laboratory Chemicals, Pergamon Press: Oxford, UK, 1980.
2. CrysAlisPro, v. 1.171.33.49b; Oxford Diffraction Ltd., 2009.
3. SMART & SAINT Software Reference Manual, Version 6.45; Bruker Analytical X-Ray Systems, Inc., Madison, 2003.
4. G. M. Sheldrick, SADABS, A software for empirical absorption correction, Ver. 2.05; University of Göttingen: Göttingen, Germany, 2002.
5. A. Altomare, G. Cascarano, C. Giacovazzo, A. Guagliardi, M. C. Burla, G. Polidori and M. Camalli, *J. Appl. Crystallogr.*, 1994, **27**, 435–435.
6. G. M. Sheldrick, A short history of SHELX. *Acta Crystallogr. A*, 2008, **64**, 112–122.

7. O. V. Dolomanov, L. J. Bourhis, R. J. Gildea, J. A. K. Howard and H. Puschmann, OLEX2: a complete structure solution, refinement and analysis program. *J. Appl. Crystallogr.*, 2009, **42**, 339–341.
8. P. Kumar, V. Kumar, S. Pandey and R. Gupta, *Dalton Trans.*, 2018, **47**, 9536–9545.
9. P. Kumar, V. Kumar and R. Gupta, *Dalton Trans.*, 2017, **46**, 10205–10209.
10. H. A. Benesi and J. H. Hildebrand, *J. Am. Chem. Soc.*, 1949, **71**, 2703–2707.
11. H. Goyal, S. Pachisia and R. Gupta, *Cryst. Growth Des.*, 2020, **20**, 6117–6128.
12. J. R. Lakowicz, Ed., Principles of Fluorescence Spectroscopy, 3rd Ed., Springer, Singapore, 2010, pp. 443–472.

List of Figures

List of Tables

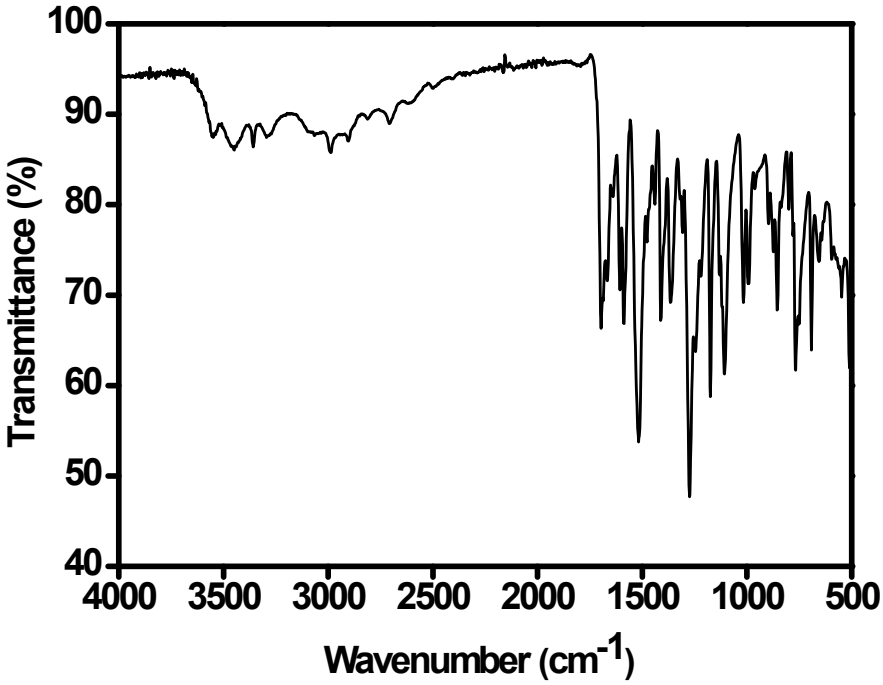

Figure S1. FTIR spectrum of **L1**.

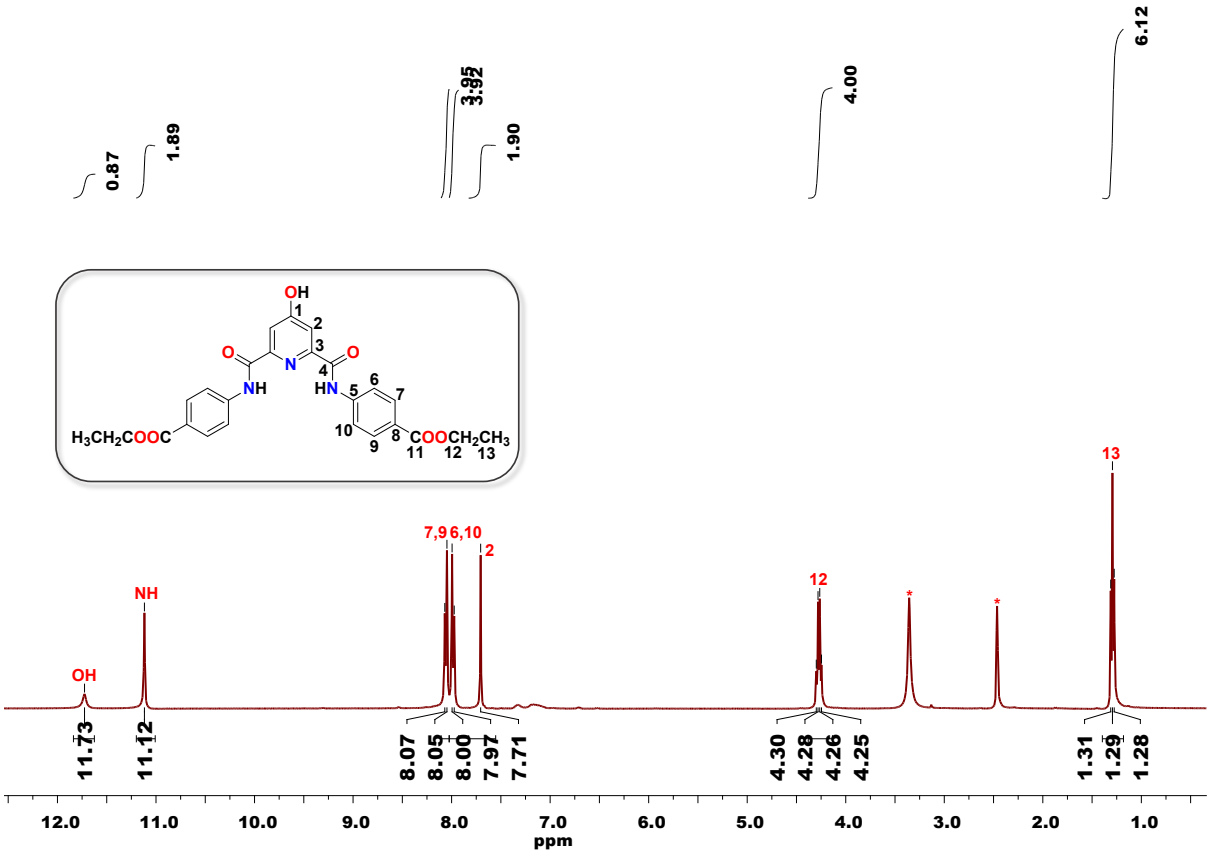

Figure S2. ^{1}H NMR spectrum of **L1** in DMSO-d_6 solvent where * represents the residual solvent and/or adventitious water peaks.

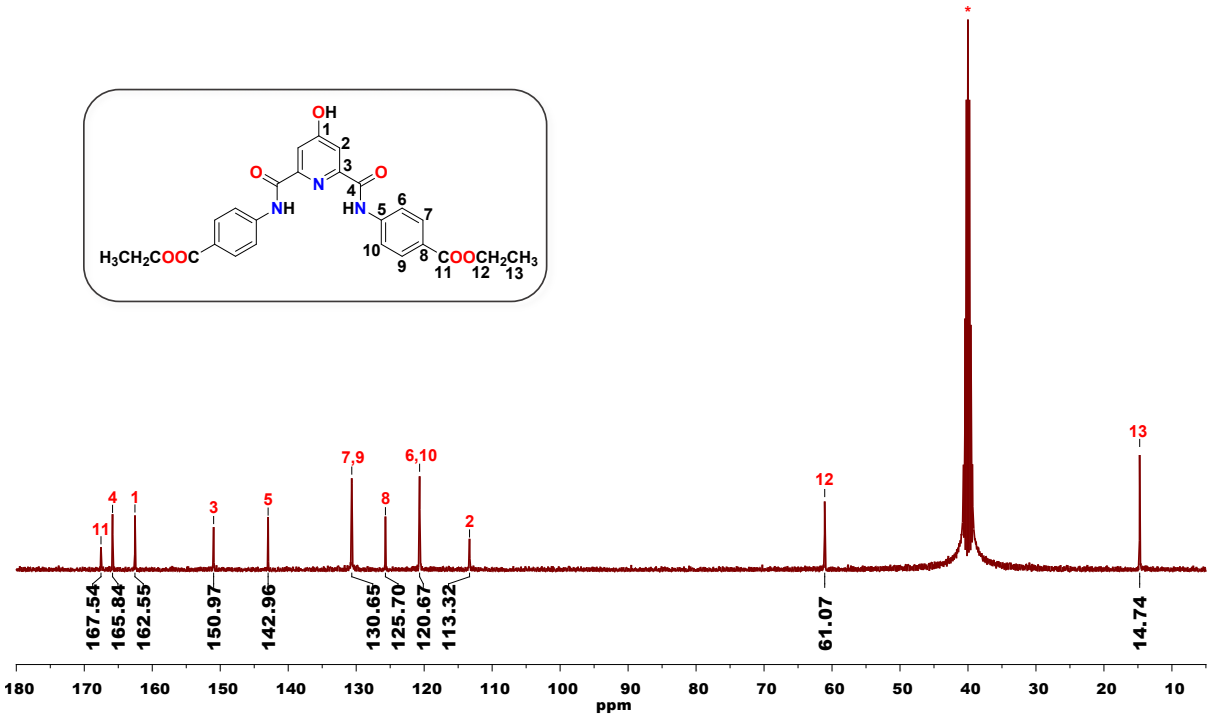

Figure S3. ^{13}C NMR spectrum of **L1** in DMSO-d_6 solvent where * represents the residual solvent peak.

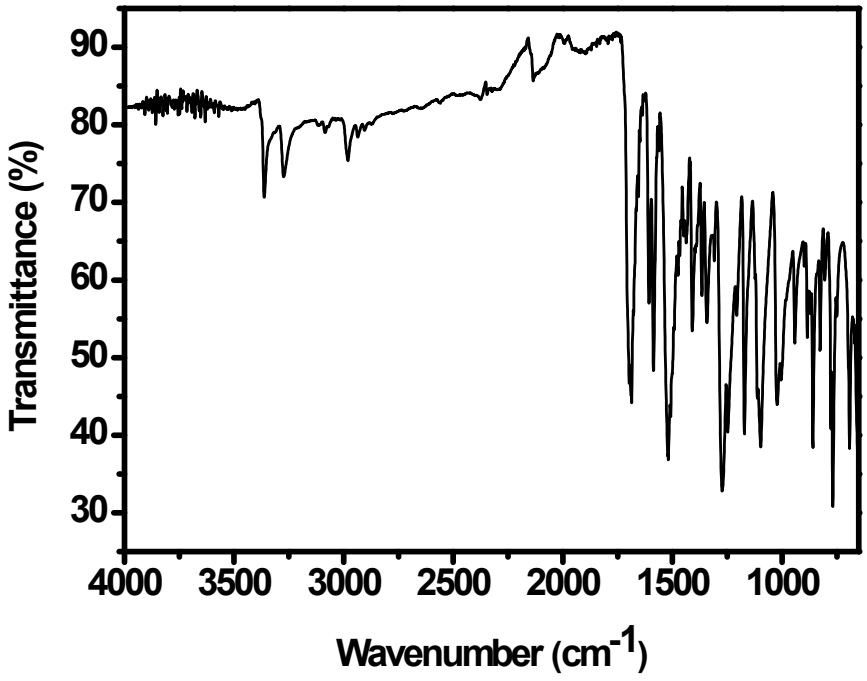

Figure S4. FTIR spectrum of **L2**.

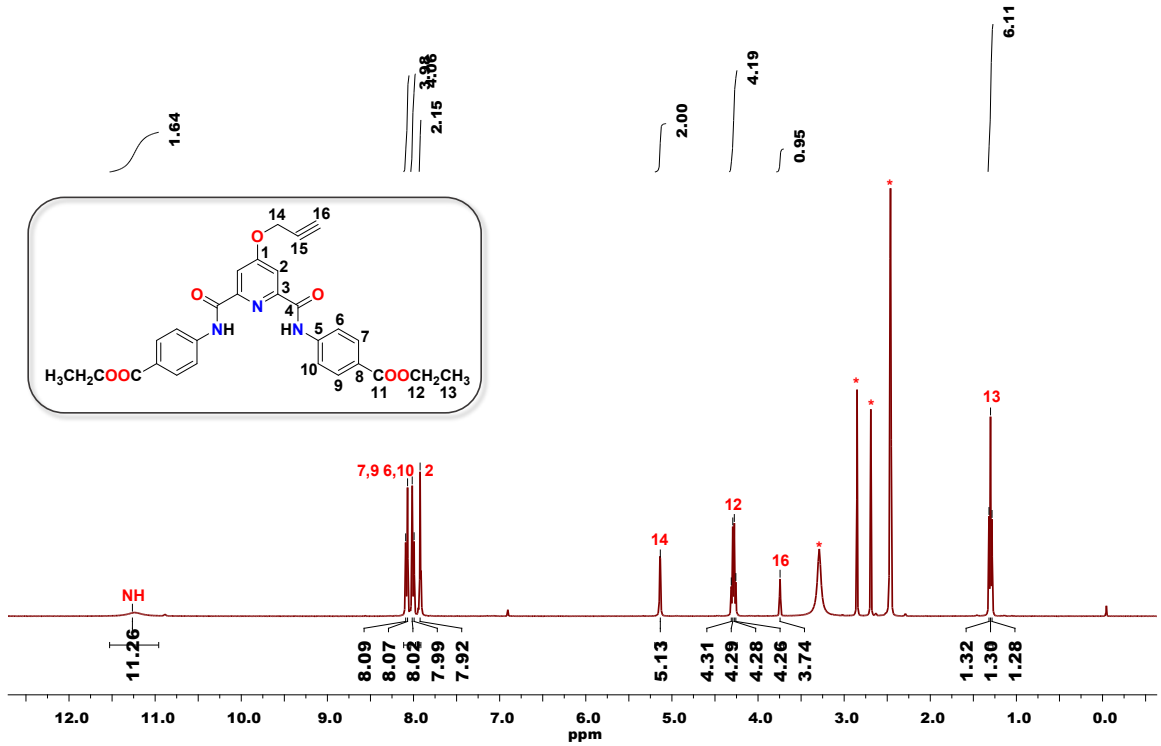

Figure S5. ^{1}H NMR spectrum of **L2** in DMSO-d_6 solvent where * represents the residual solvent and/or adventitious water peaks.

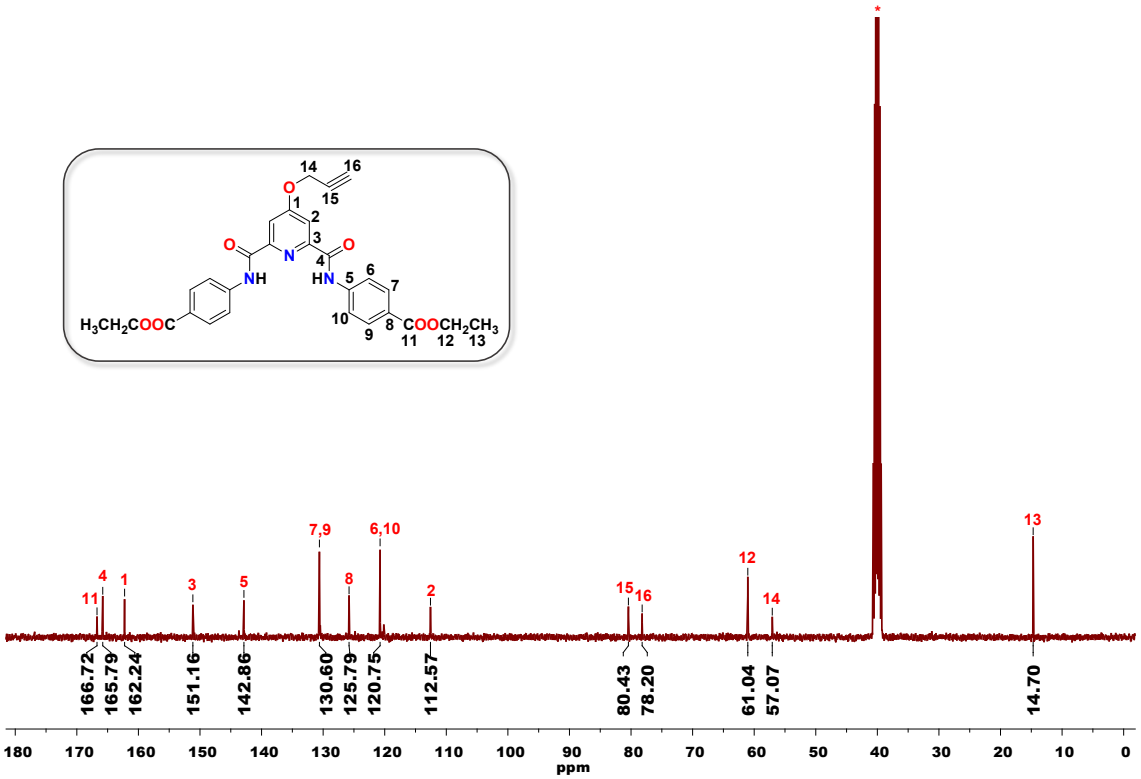

Figure S6. ^{13}C NMR spectrum of **L2** in DMSO-d_6 solvent where * represents the residual solvent peak.

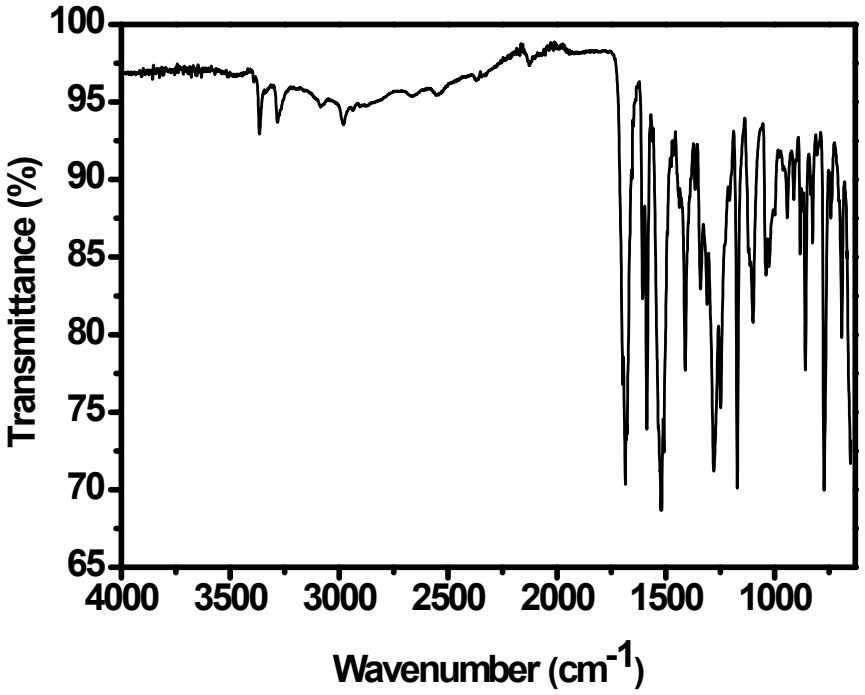

Figure S7. FTIR spectrum of ligand **L3**.

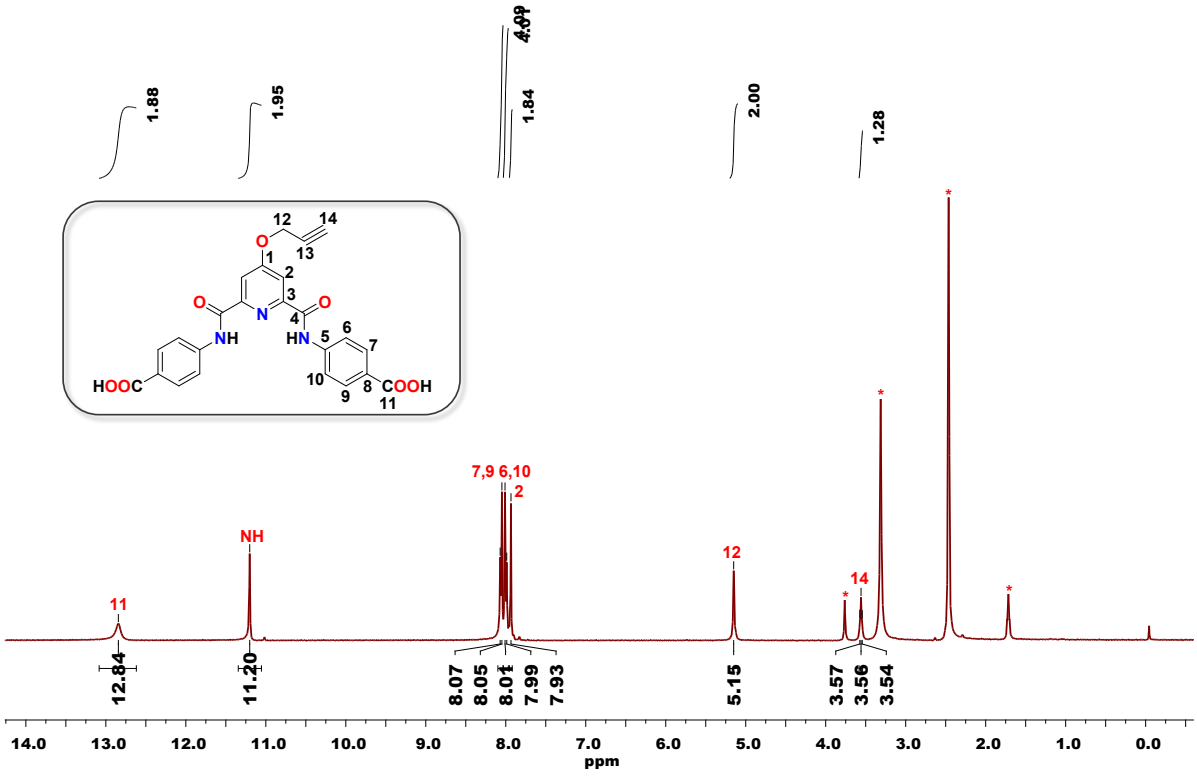

Figure S8. ^{1}H NMR spectrum of ligand **L3** in DMSO-d_6 solvent where * represents the residual solvent and/or adventitious water peaks.

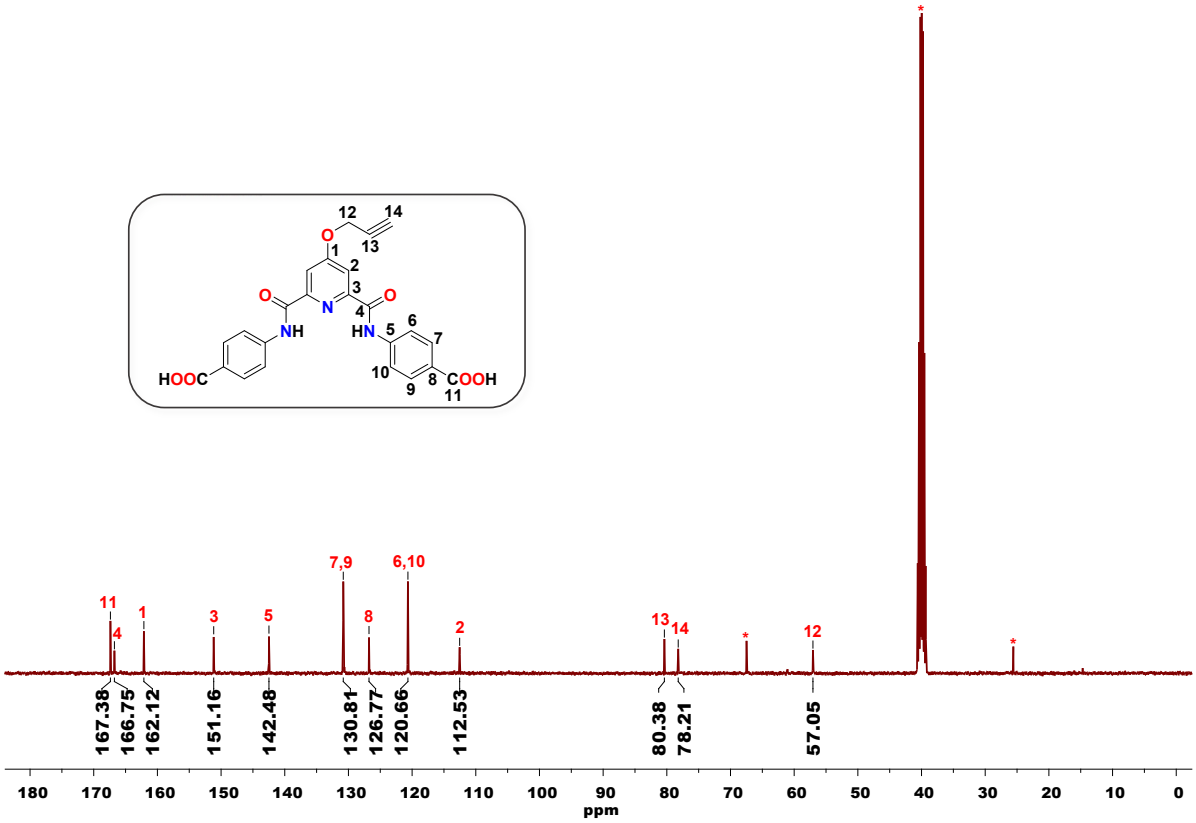

Figure S9. ^{13}C NMR spectrum of ligand **L3** in DMSO-d_6 solvent where * represents the residual and/or adventitious solvent peaks.

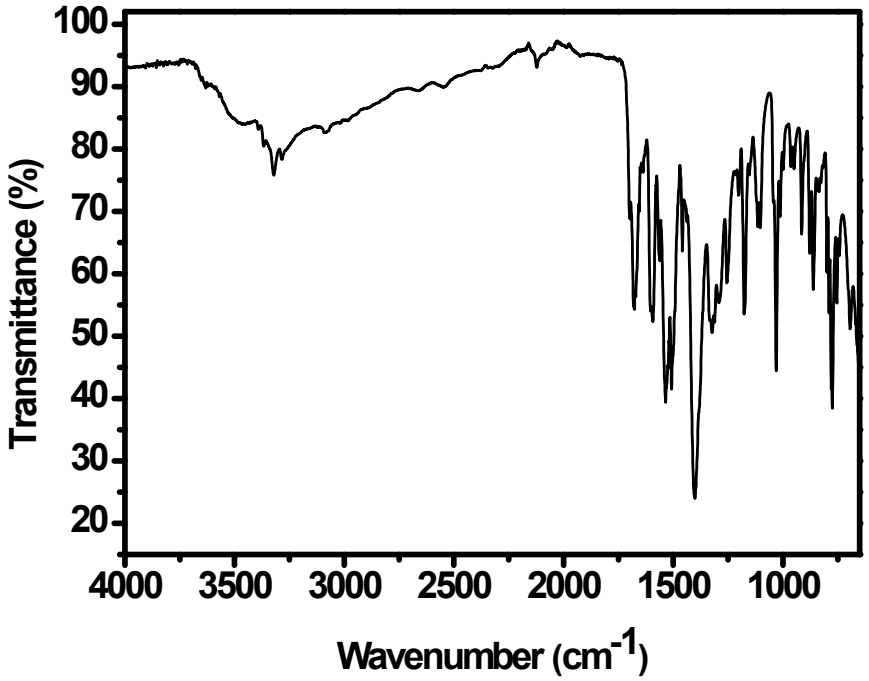

Figure S10. FTIR spectrum of MOF **1**.

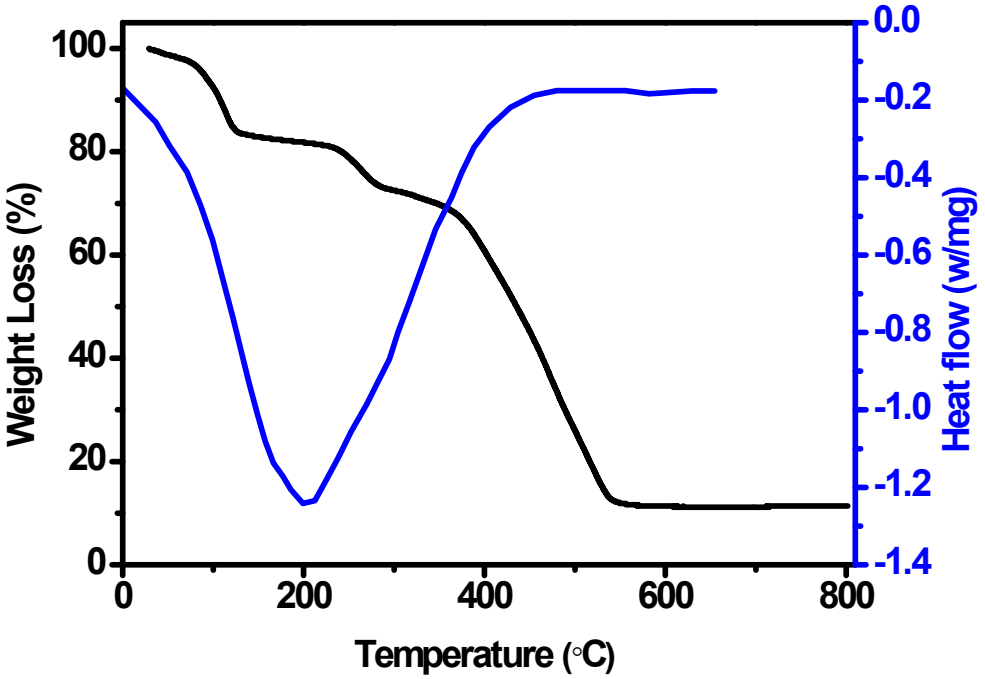

Figure S11. Thermal Gravimetric Analysis (TGA, black trace) and Differential Scanning Calorimetric (DSC, blue trace) plots for MOF **1**.

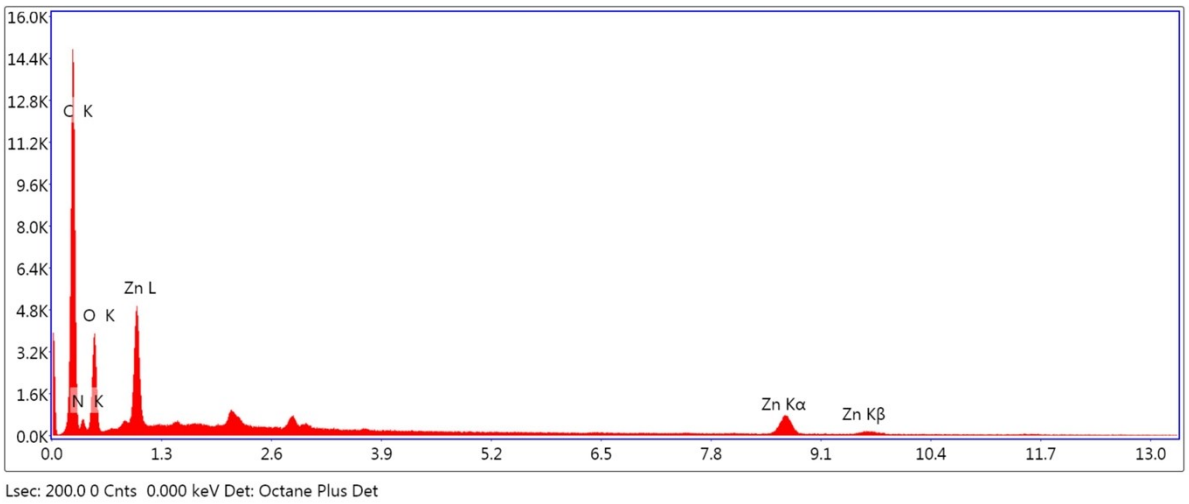

Figure S12. EDX spectrum of MOF **1**.

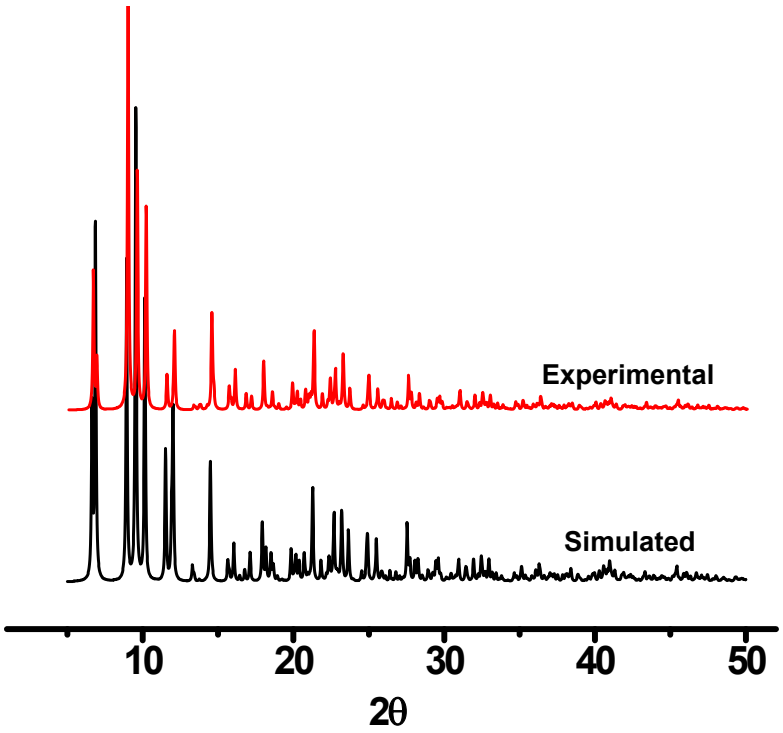

Figure S13. X-ray powder diffraction patterns for as-synthesized MOF **1** (red trace) and the one simulated from Mercury 3.0 using the single crystal diffraction data (black trace).

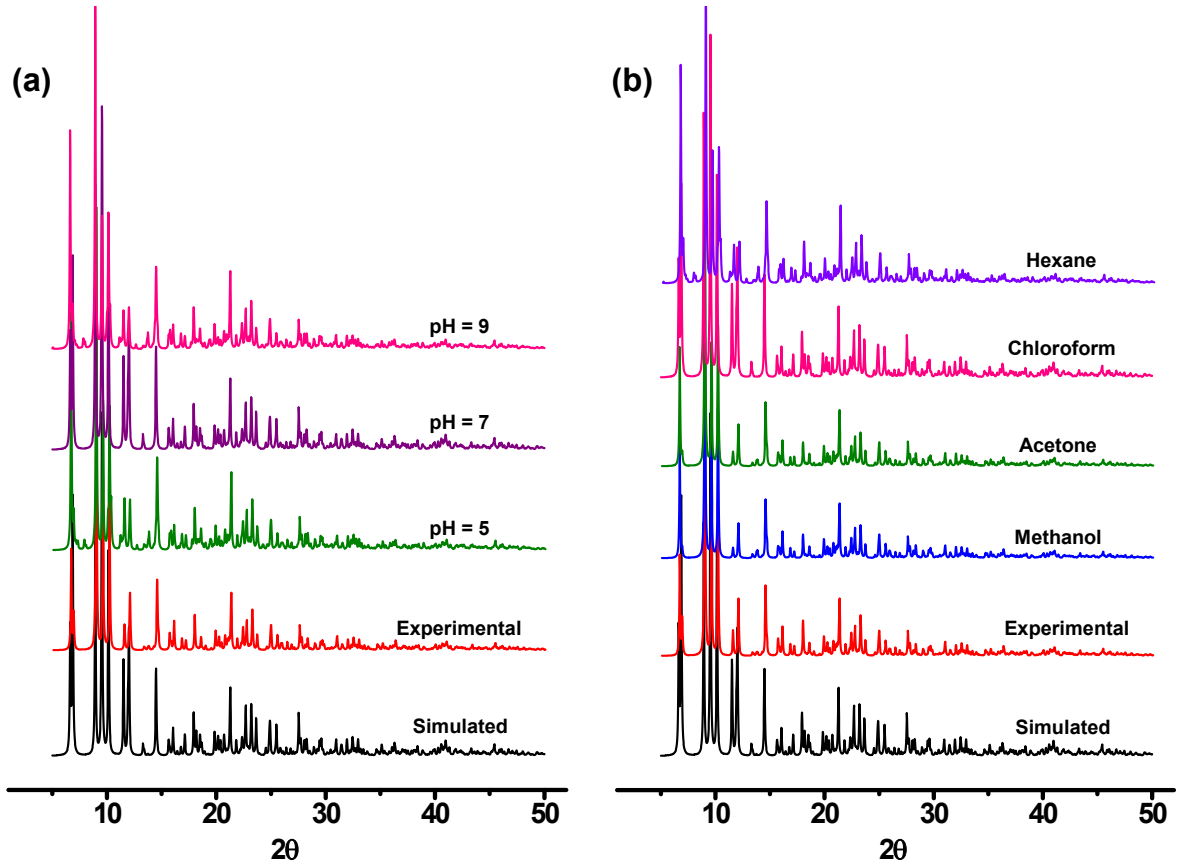

Figure S14. (a) X-ray powder diffraction patterns of as-synthesized MOF **1**, its simulated patterns, and after treatment in different (a) pHs and (b) organic solvents.

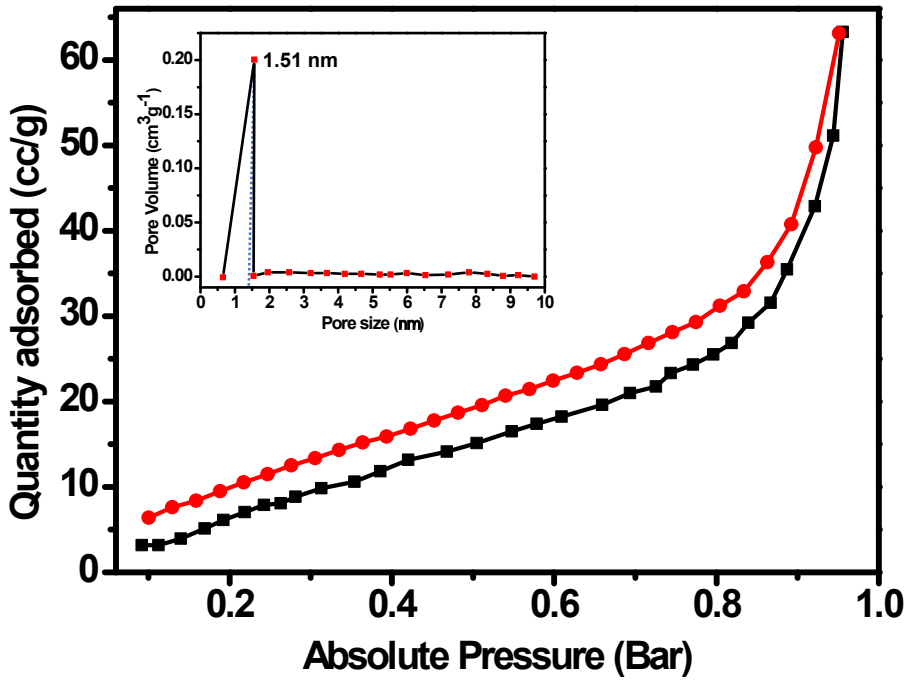

Figure S15. N_2 sorption isotherm measured for MOF **1** at 77 K. Black and red traces respectively denote sorption and desorption plots. Inset shows the pore size distribution plot.

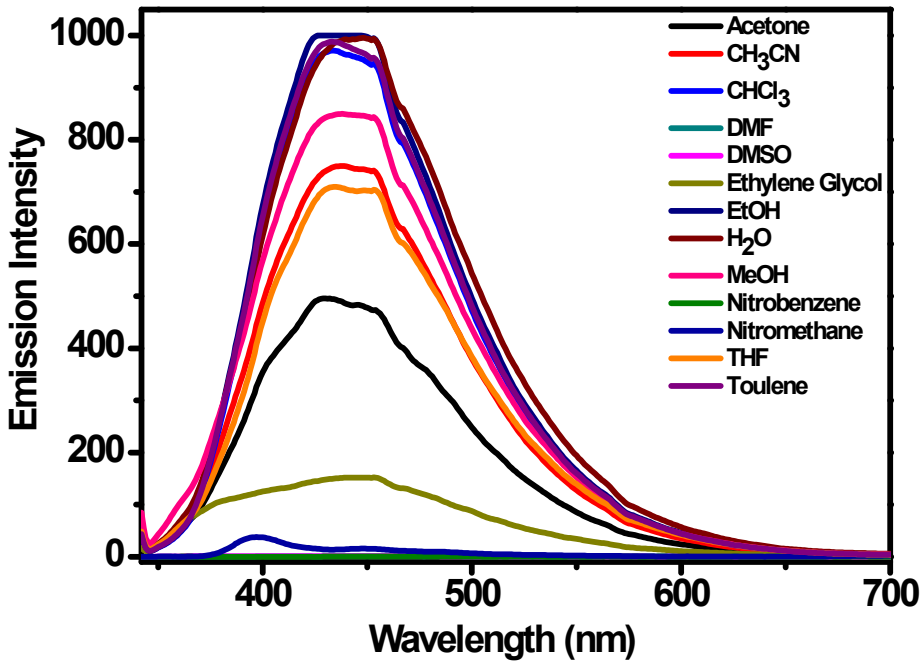

Figure S16. Emission spectra of MOF **1** recorded in different solvents.

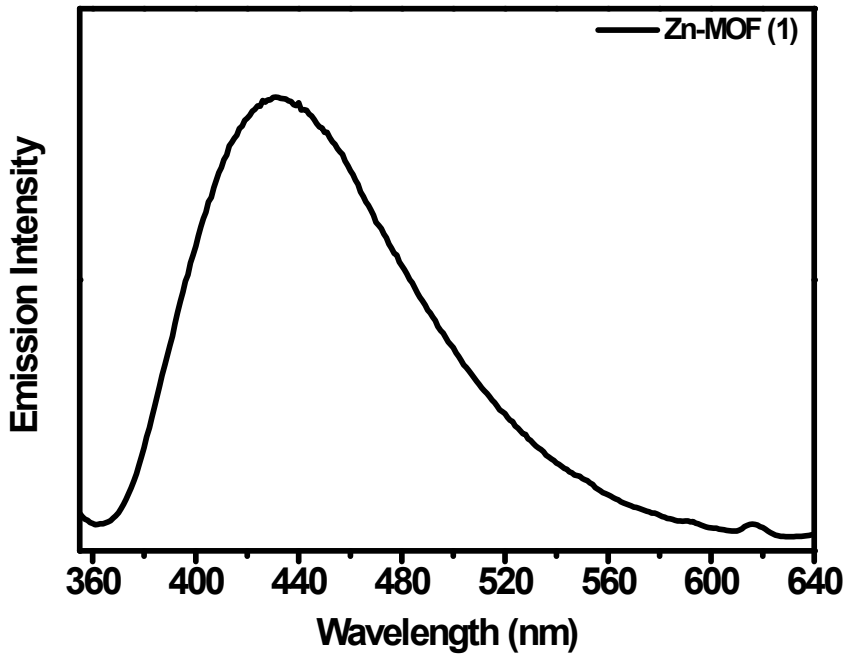

Figure S17. Solid-state fluorescence spectrum of MOF **1**.

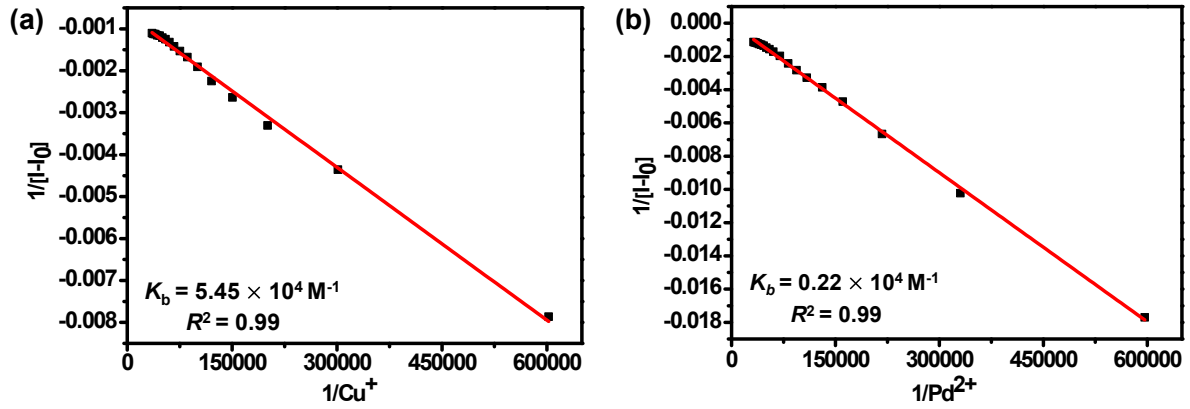

Figure S18. Determination of binding constants by Benesi-Hildebrand plots for the detection of (a) Cu^{+} and (b) Pd^{2+} ion by **1** from the emission spectral profiles.

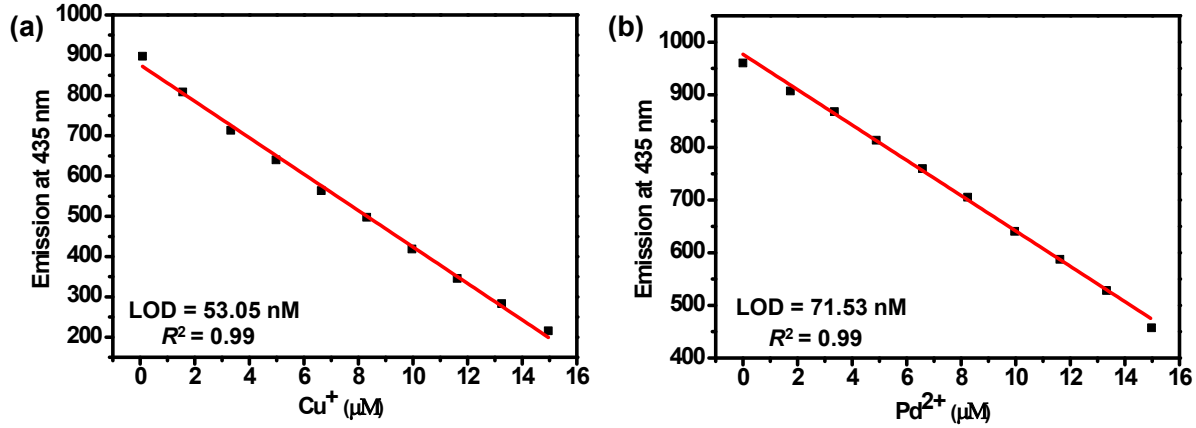

Figure S19. Determination of detection limits for (a) Cu^{+} and (b) Pd^{2+} ions by **1** from the emission spectral titrations.

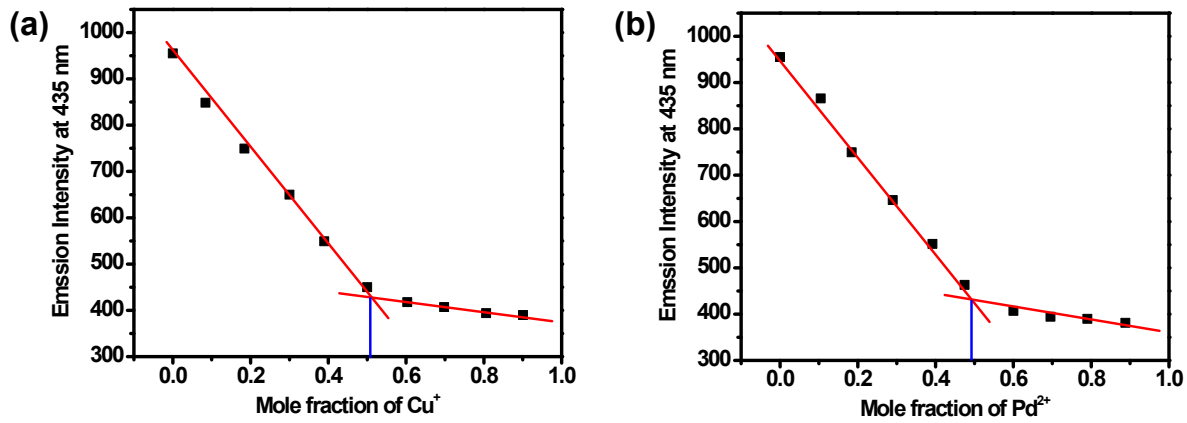

Figure S20. Job's plot showing a 1:1 stoichiometry of **1** towards (a) Cu^{+} and (b) Pd^{2+} ions.

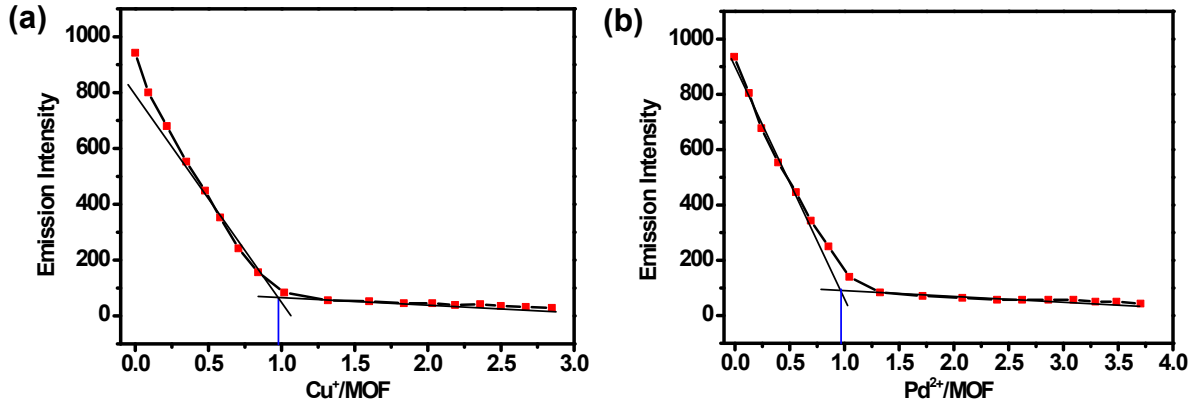

Figure S21. Mole ratio method showing a 1:1 stoichiometry of **1** towards (a) Cu^{+} and (b) Pd^{2+} ions.

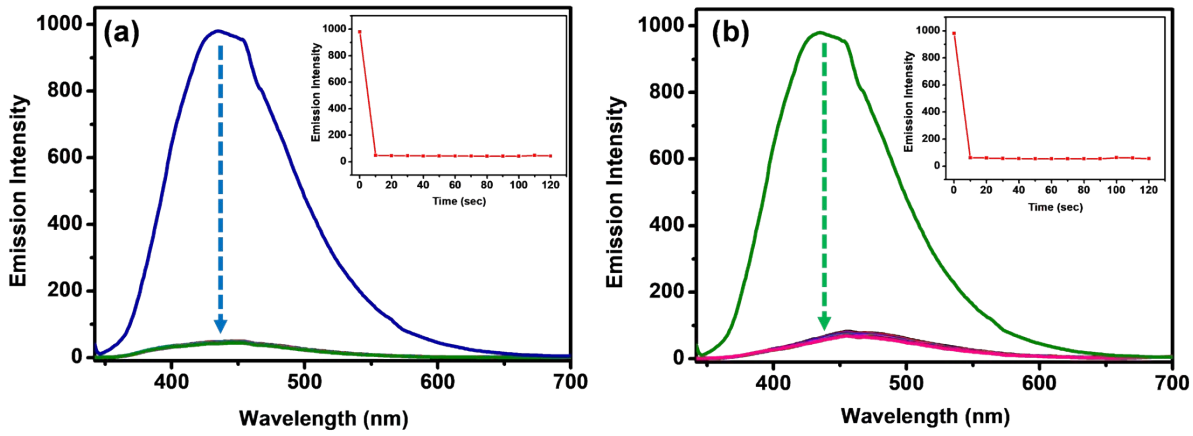

Figure S22. Change in the emission spectra of **1** as a function of time in the presence of (a) Cu^{+} ion (28 μM) and (b) Pd^{2+} ion (32 μM). Both insets show the response time of **1** for the detection of Cu^{+} and Pd^{2+} ions, respectively.

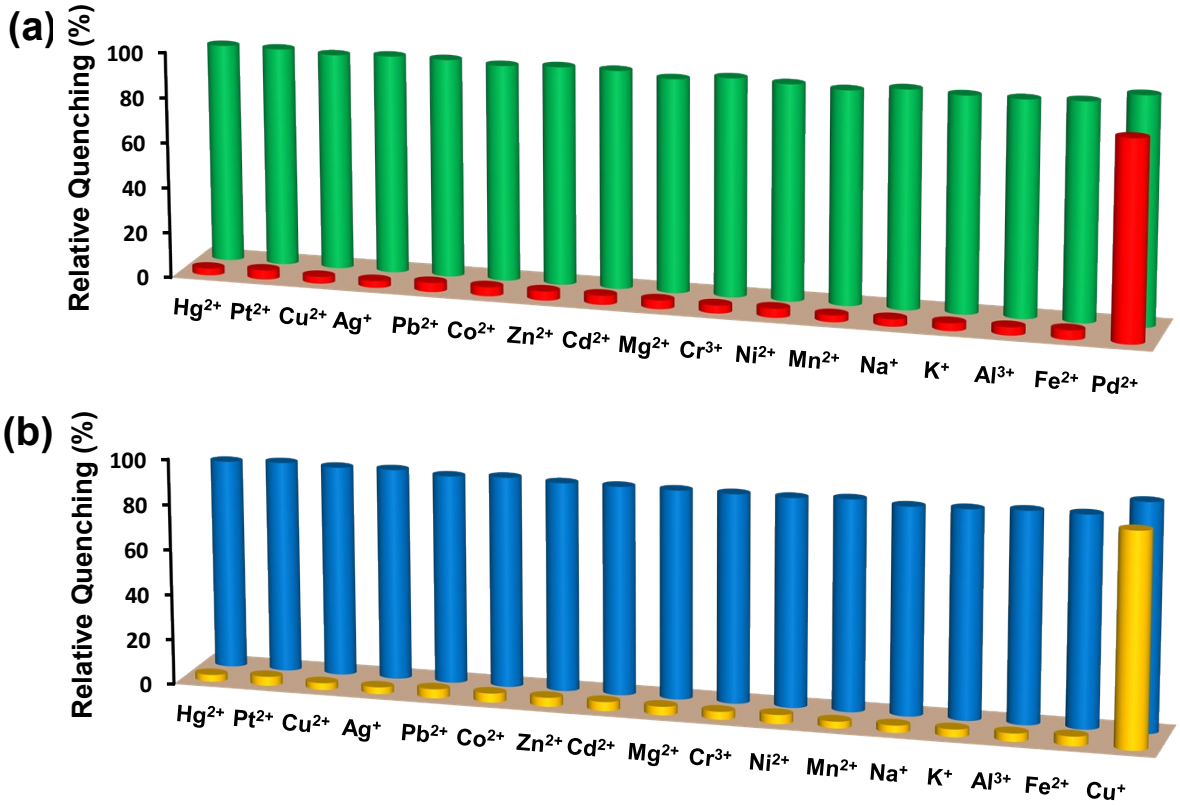

Figure S23. (a) Selectivity of **1** toward Cu^{+} ion in the presence of other metal ions: **1** + metal ions (red pillars) and **1** + metal ions + Cu^{+} ion (green pillars). (b) Selectivity of **1** toward Pd^{2+} ion in the presence of other metal ions: **1** + metal ions (yellow pillars) and **1** + metal ions + Pd^{2+} ion (blue pillars). All studies were performed in an aqueous medium.

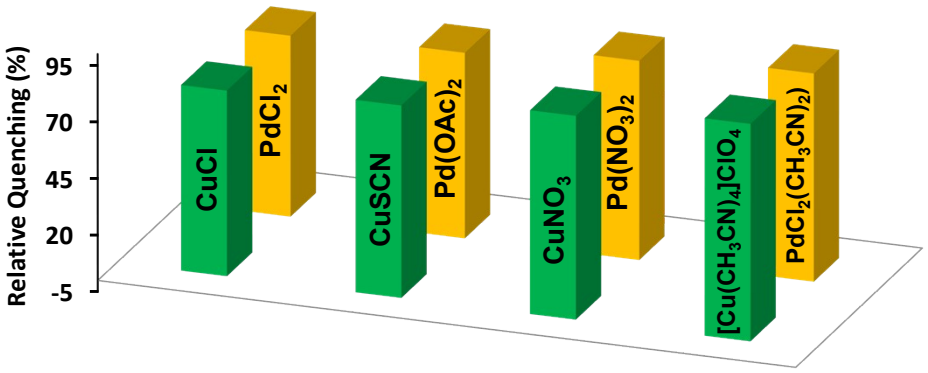

Figure S24. Quenching efficiency of MOF **1** towards Cu^{+} ion (28 μM, green pillars) and Pd^{2+} ion (32 μM, orange pillars) having different anions.

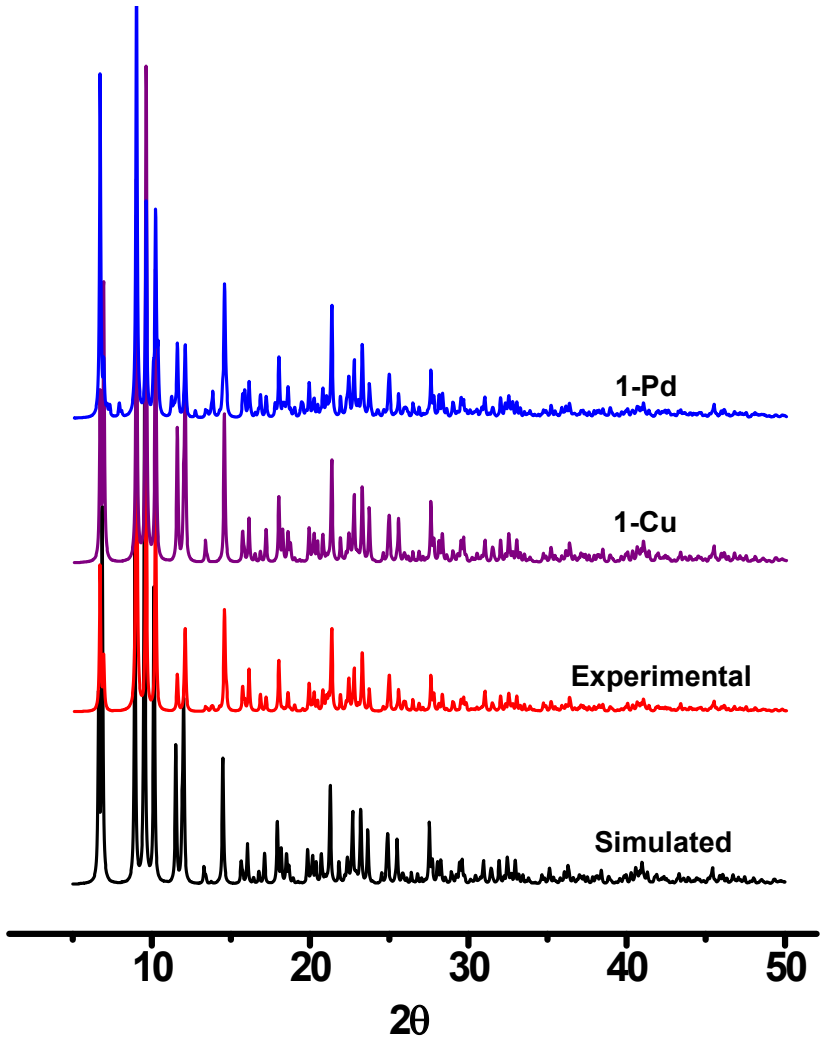

Figure S25. X-ray powder diffraction patterns for as-synthesized **1** (red trace); its simulated one (black trace); and after reaction with Cu^{+} (purple trace) and Pd^{2+} (blue trace) ions.

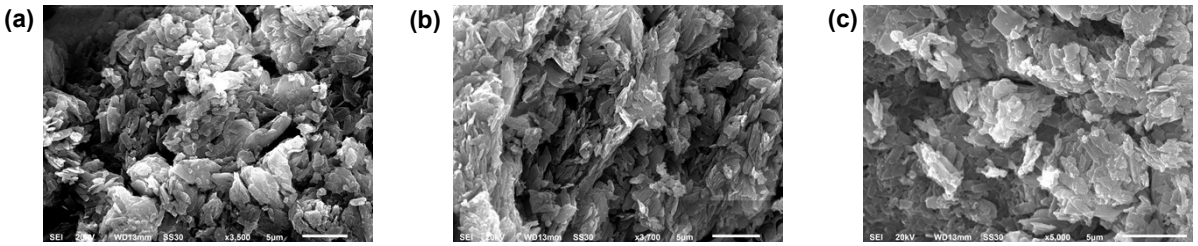

Figure S26. SEM images of (a) MOF **1**, (b) **1**-Cu and (c) **1**-Pd.

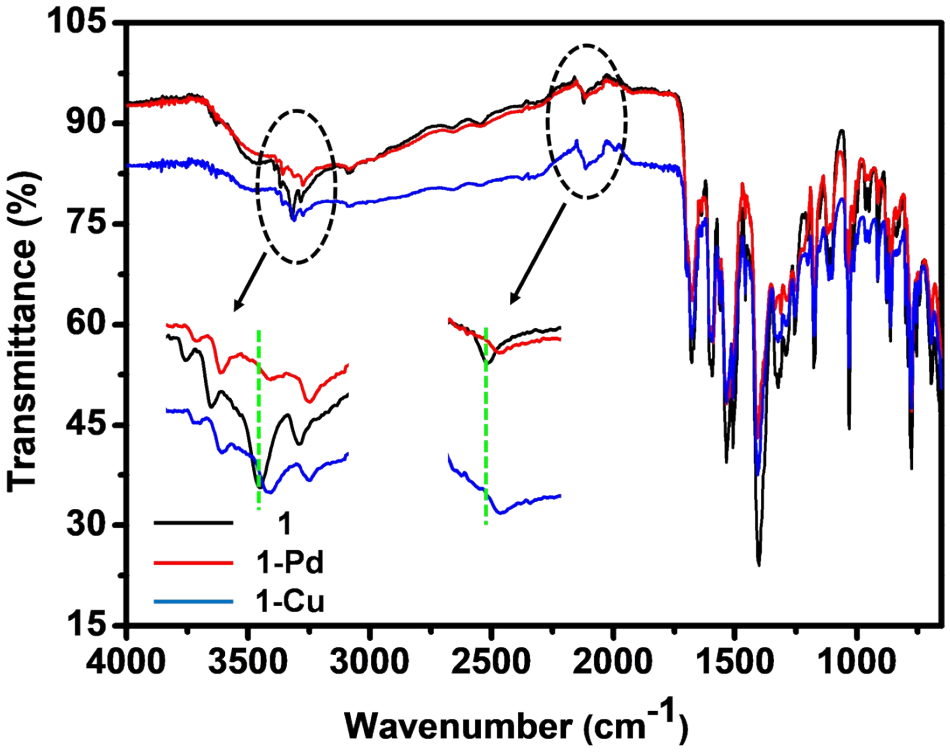

Figure S27. FTIR spectra of MOF **1** (black trace), **1-Cu** (blue trace) and **1-Pd** (red trace).

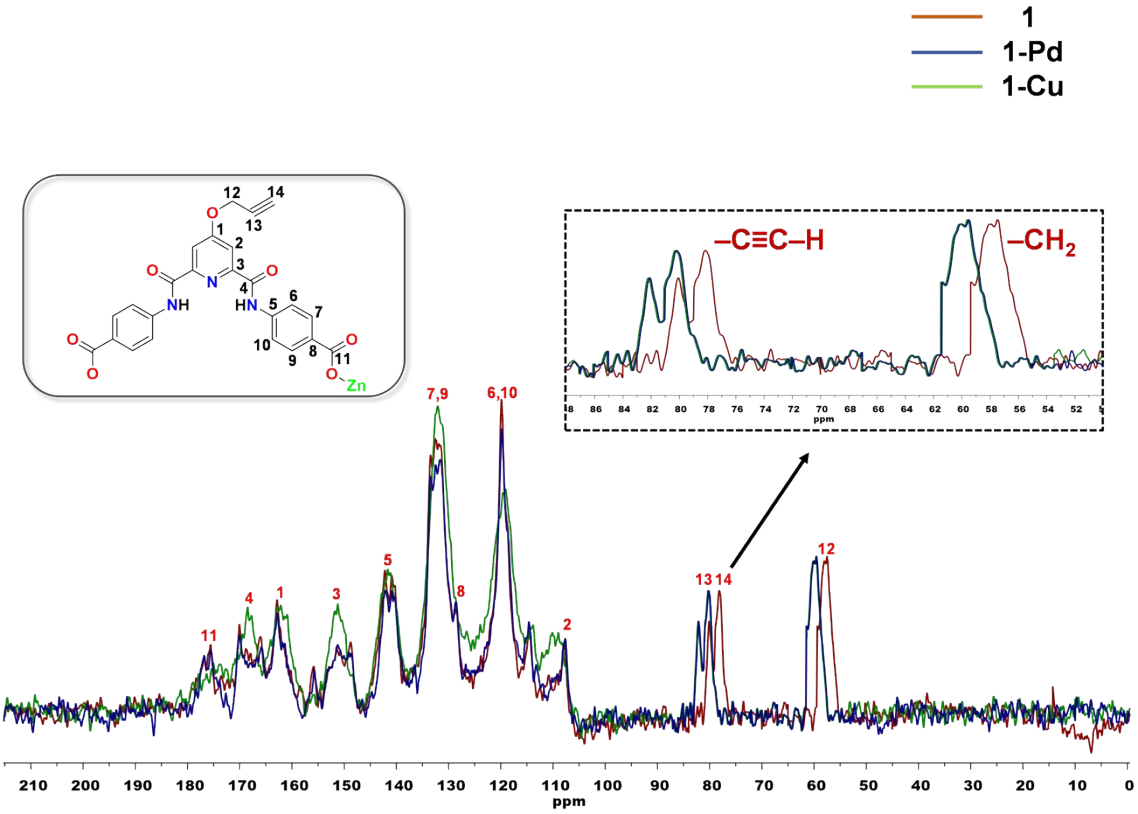

Figure S28. Solid-state ^{13}C NMR spectra of **1** in the absence (brown trace) and presence of 5 equiv. of Cu^{+} (green trace) and Pd^{2+} (blue trace) ions.

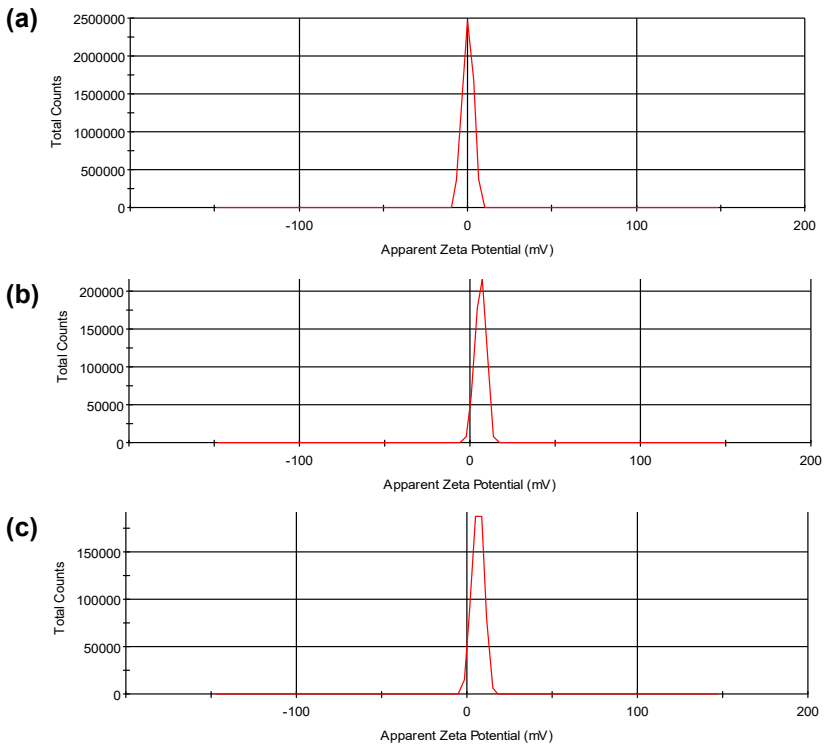

Figure S29. ζ potential plots for (a) **1**, (b) **1**-Pd and (c) **1**-Cu.

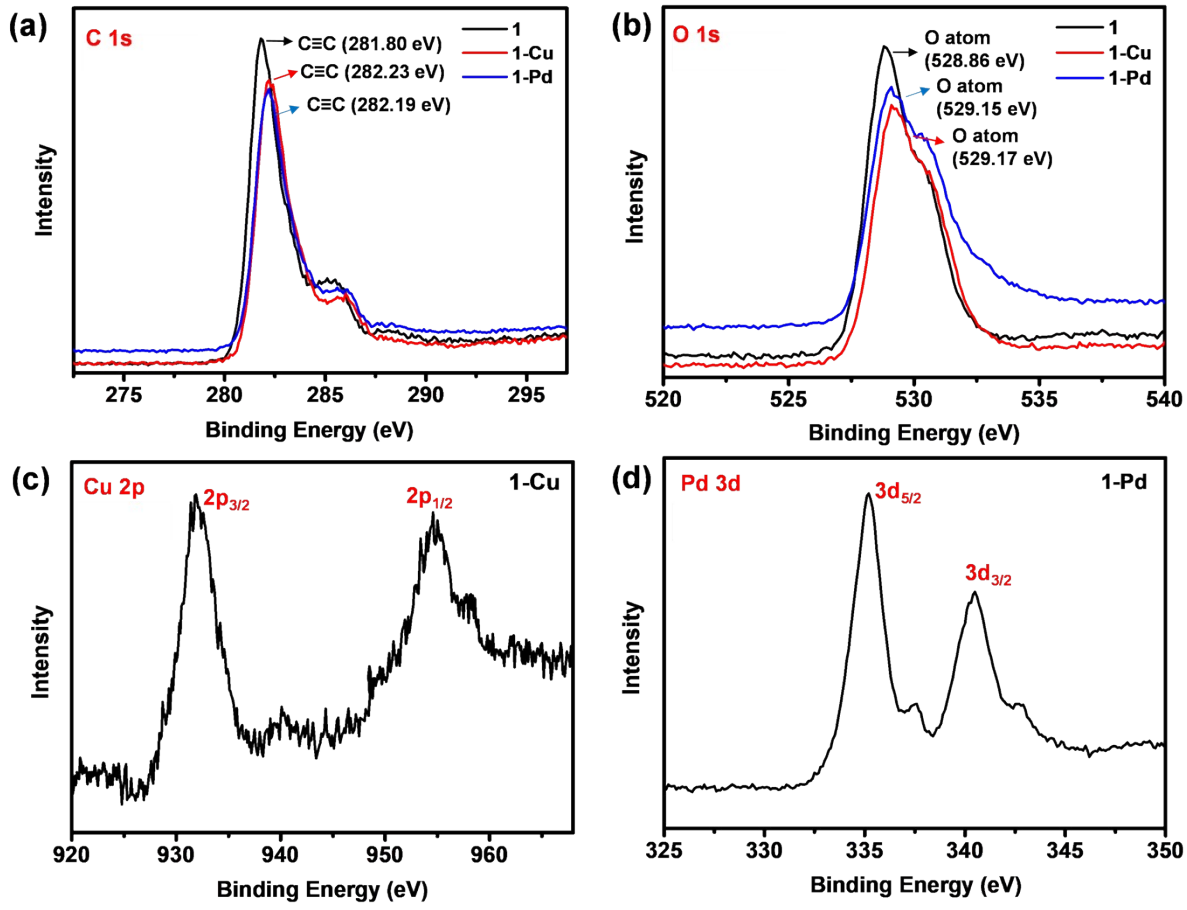

Figure S30. XPS spectra of (a) **1**, **1**-Cu and **1**-Pd showing C1s region. (b) **1**, **1**-Cu and **1**-Pd showing O1s region. (c) **1**-Cu showing Cu2p region. (d) **1**-Pd showing Pd3d region.

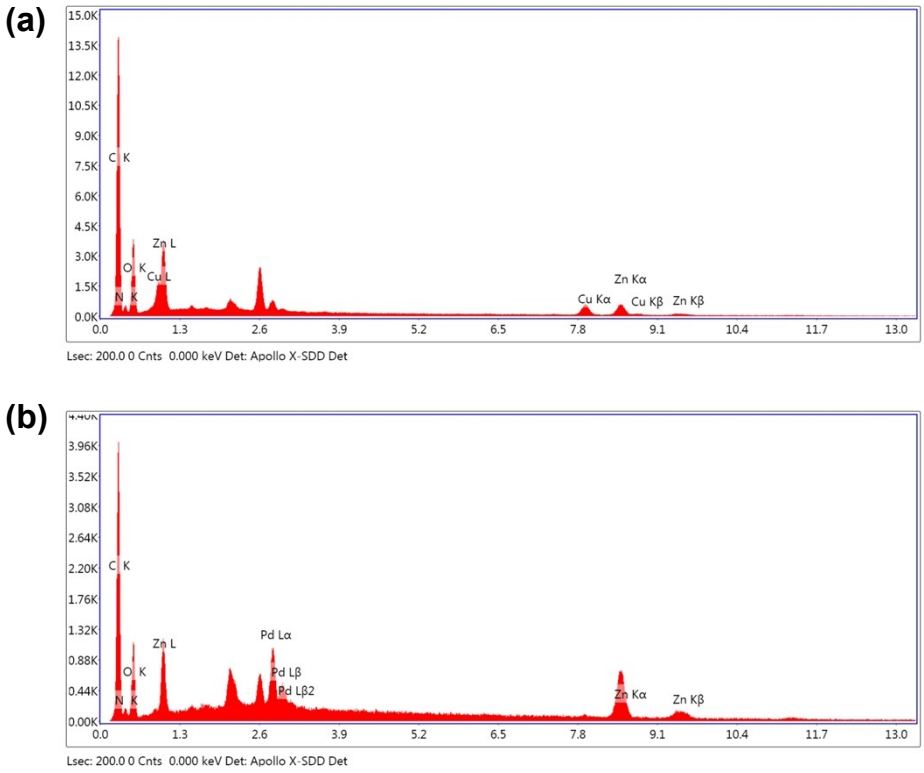

Figure S31. EDX spectra for (a) **1**-Cu and (b) **1**-Pd.

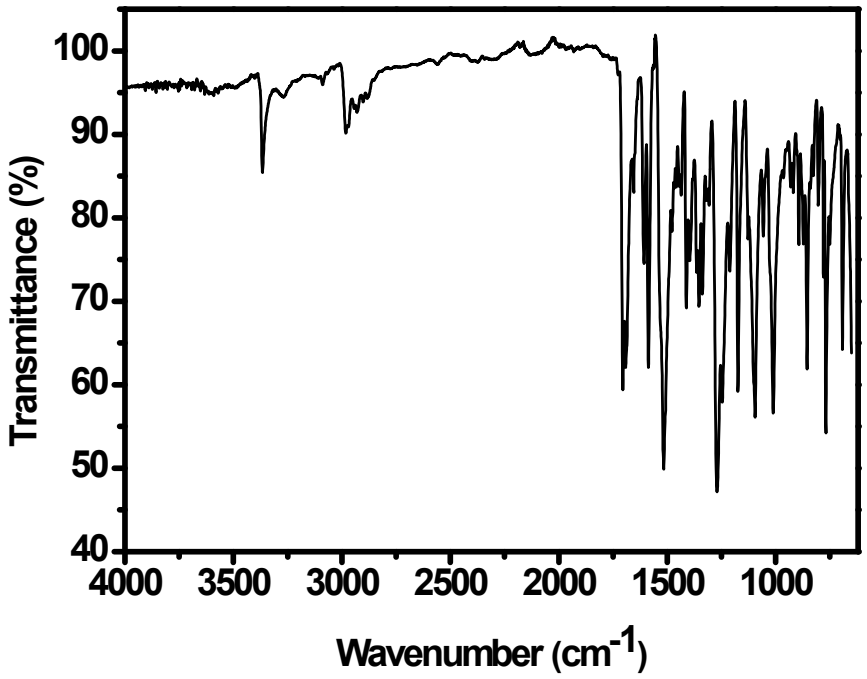

Figure S32. FTIR spectrum of **L4**.

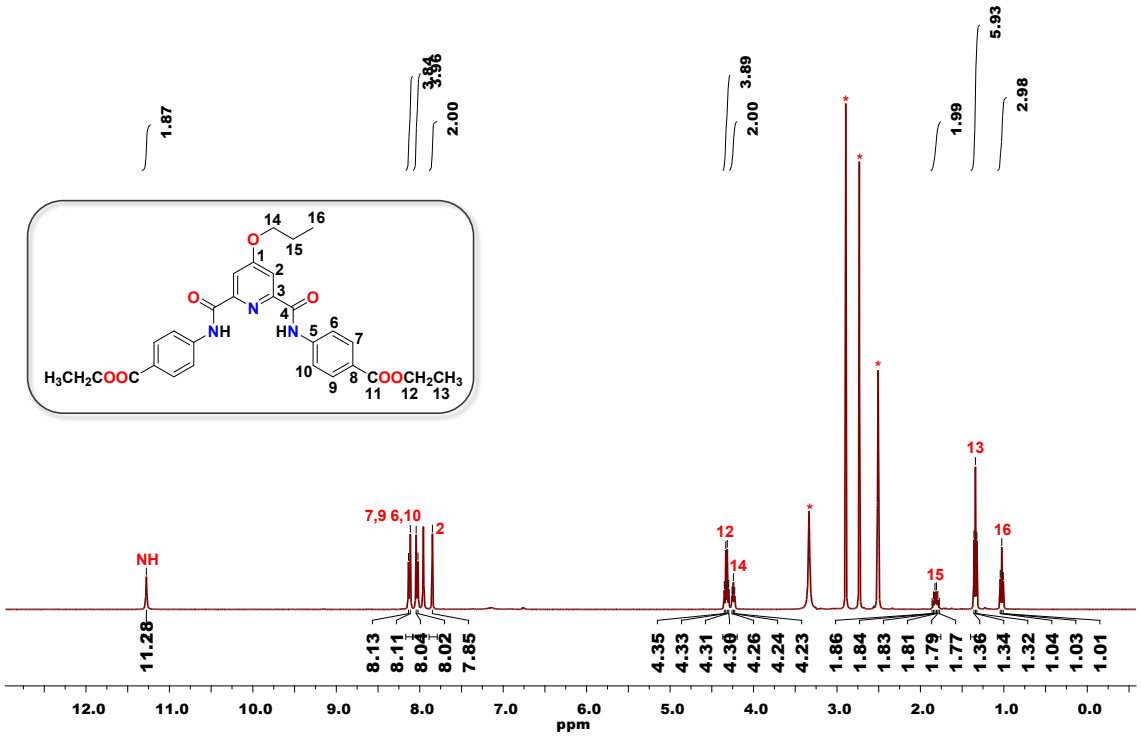

Figure S33. ^{1}H NMR spectrum of **L4** in DMSO-d_6 solvent where * represents the residual solvent and/or adventitious water peaks.

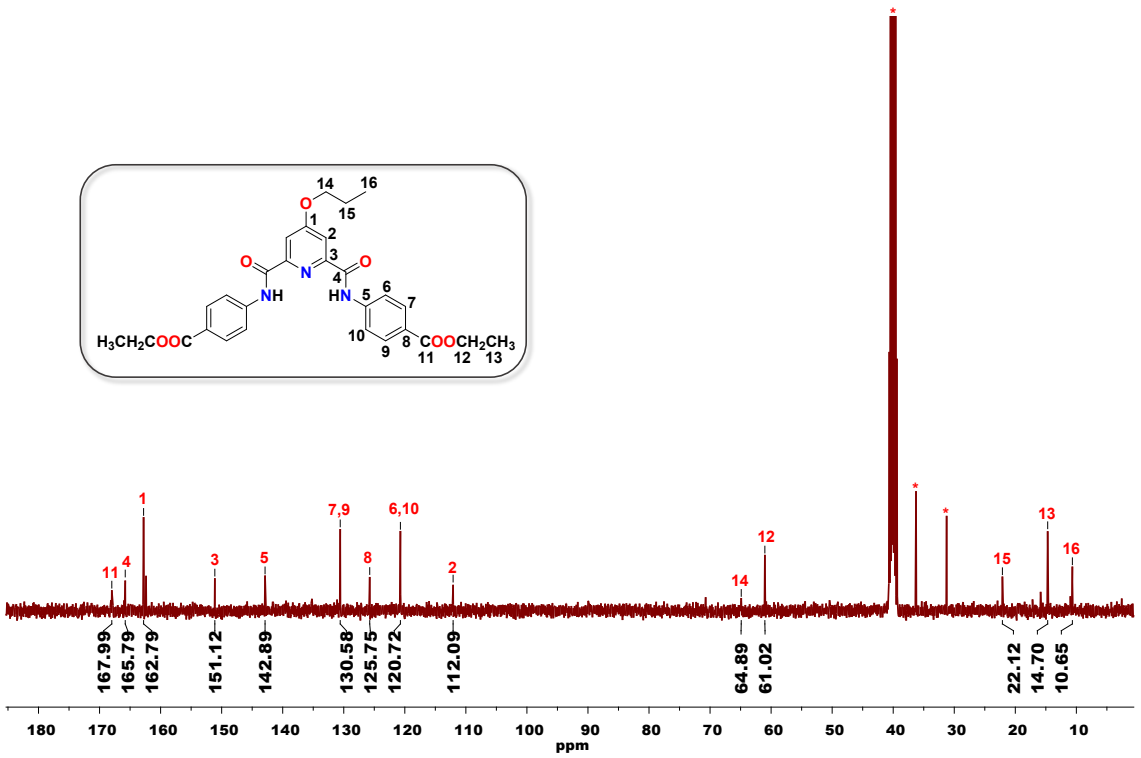

Figure S34. ^{13}C NMR spectrum of **L4** in DMSO-d_6 solvent where * represents the residual and/or adventitious solvent peaks.

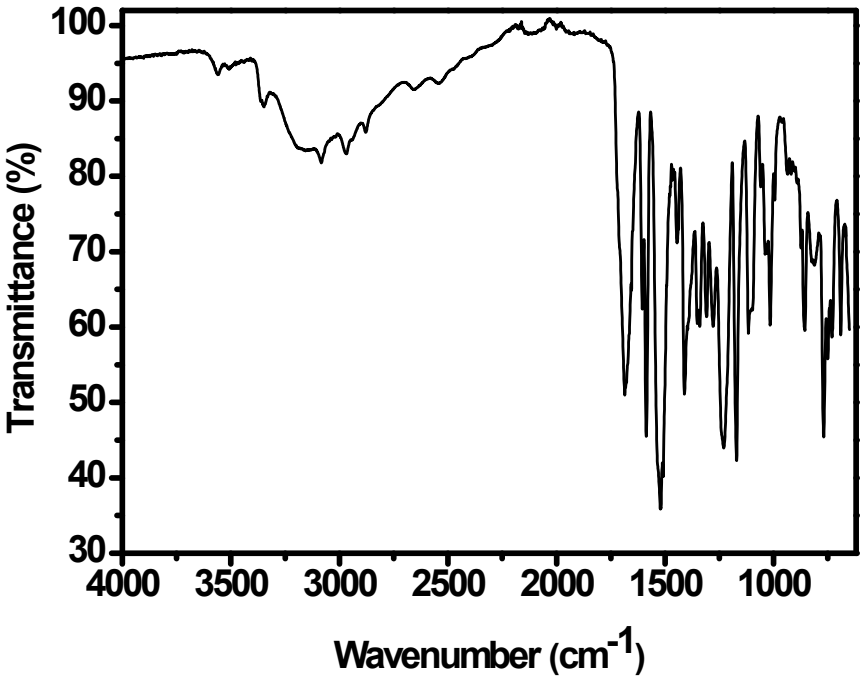

Figure S35. FTIR spectrum of ligand **L5**.

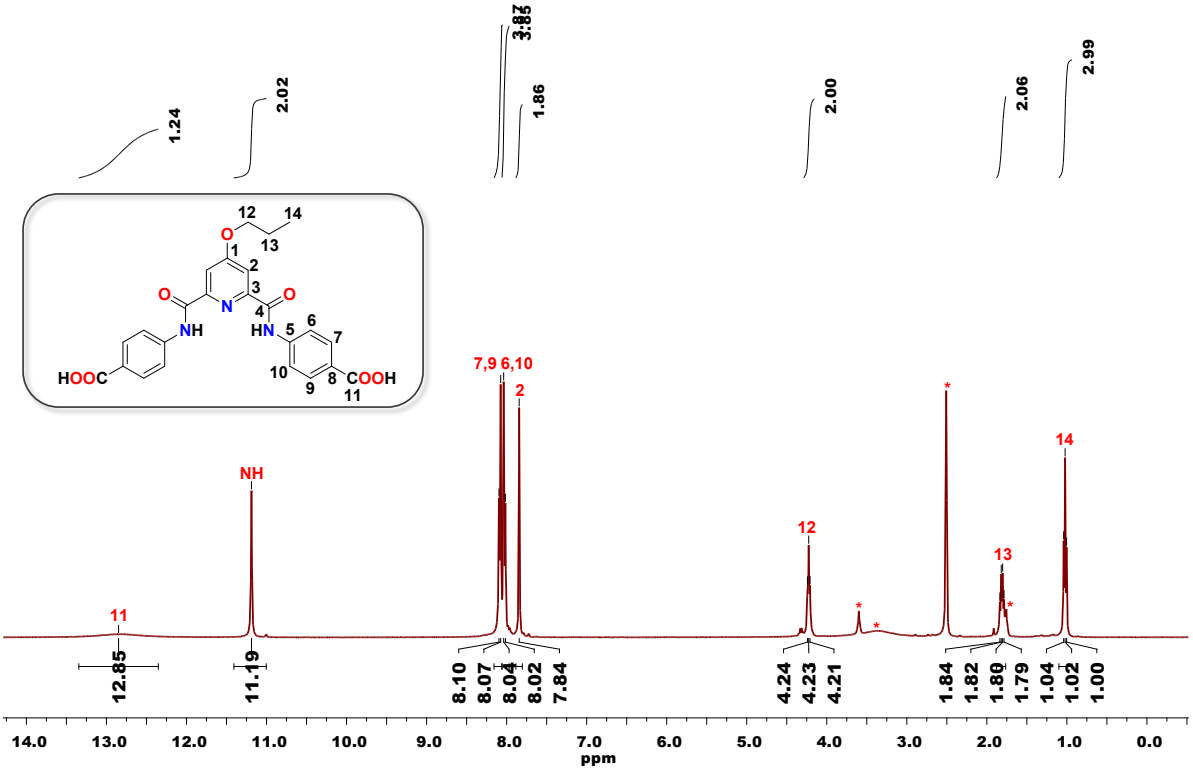

Figure S36. ^{1}H NMR spectrum of ligand **L5** in DMSO-d_6 solvent where * represents the residual solvent and/or adventitious water peaks.

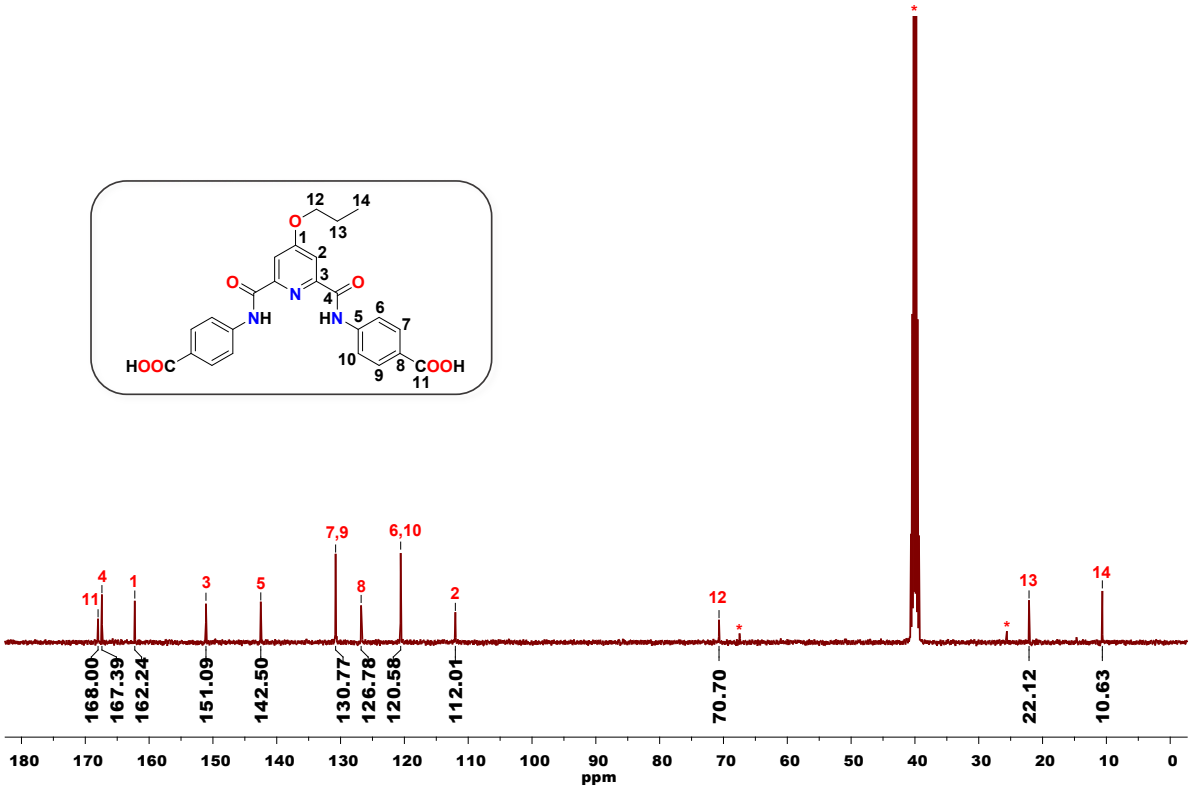

Figure S37. ^{13}C NMR spectrum of ligand **L5** in DMSO-d_6 solvent where * represents the residual and/or adventitious solvent peaks.

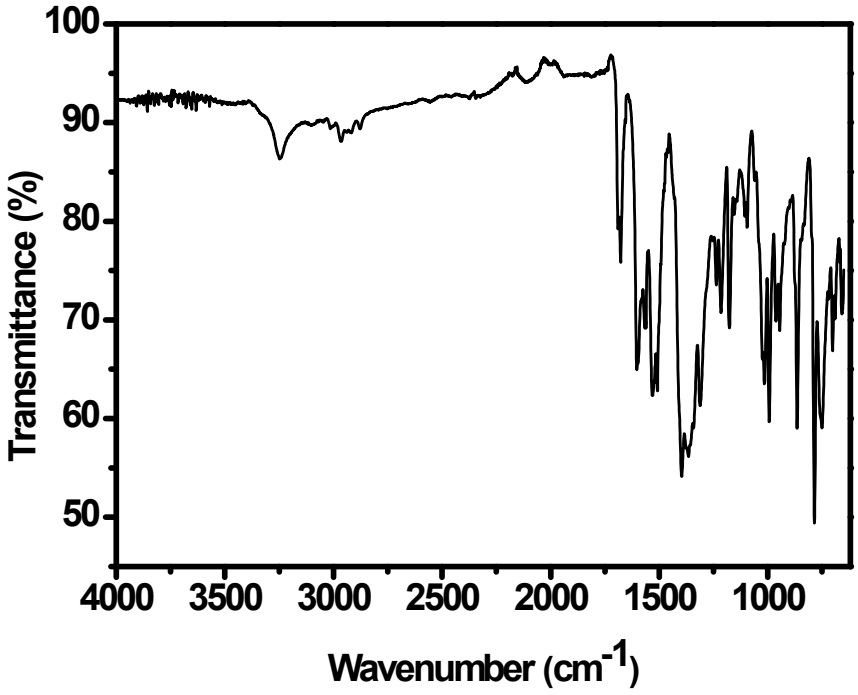

Figure S38. FTIR spectrum of MOF **2**.

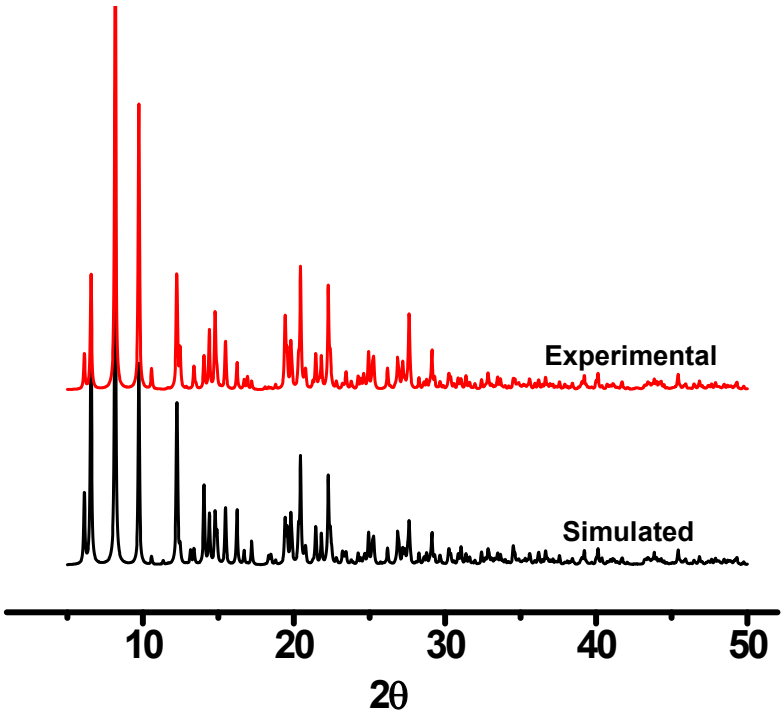

Figure S39. X-ray powder diffraction patterns for as-synthesized MOF **2** (red trace) and the one simulated from Mercury 3.0 using the single crystal diffraction data (black trace).

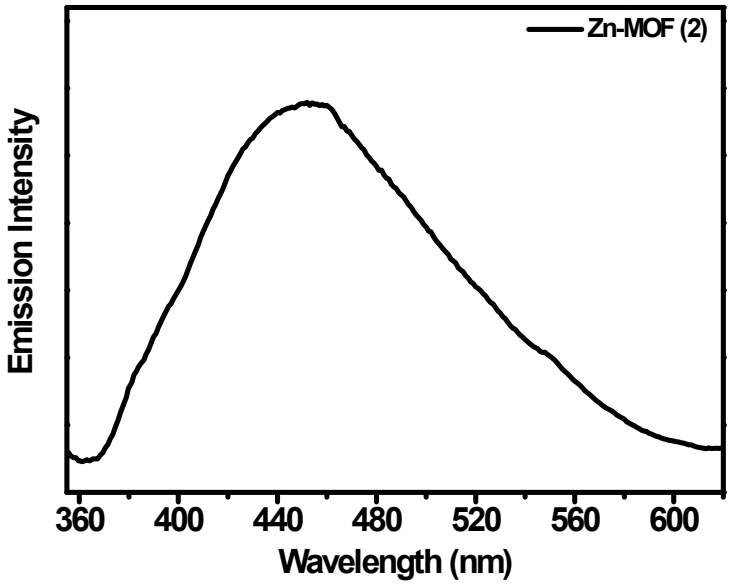

Figure S40. Solid-state fluorescence spectrum of MOF **2**.

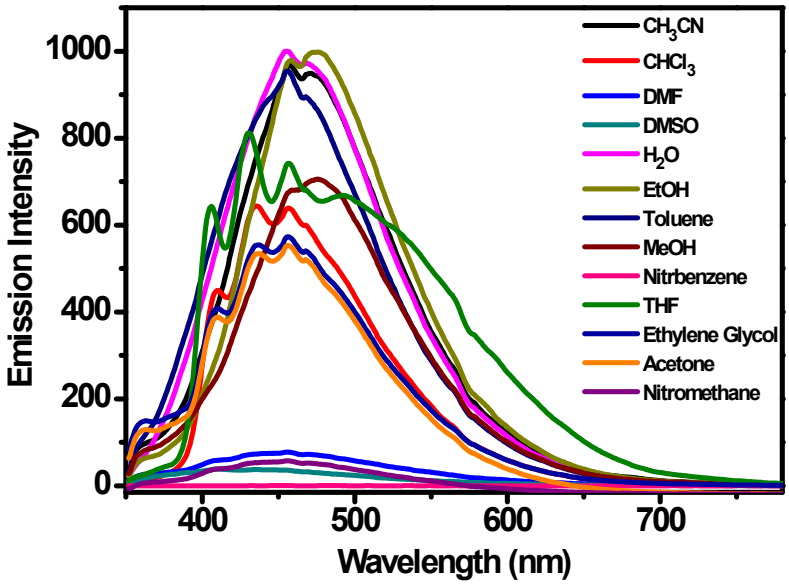

Figure S41. Emission spectra of MOF **2** recorded in different solvents.

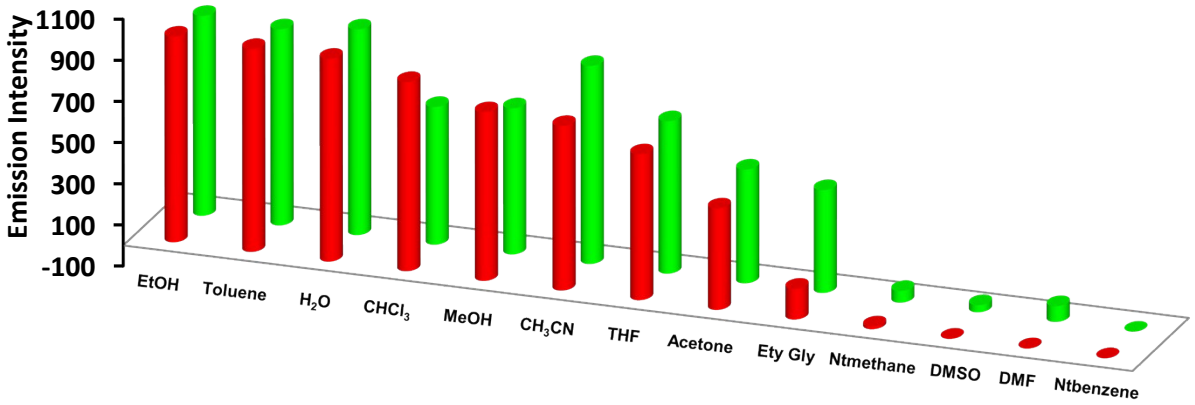

Figure S42. Bar diagram showing relative emission intensity of MOFs **1** and **2** in different solvents.

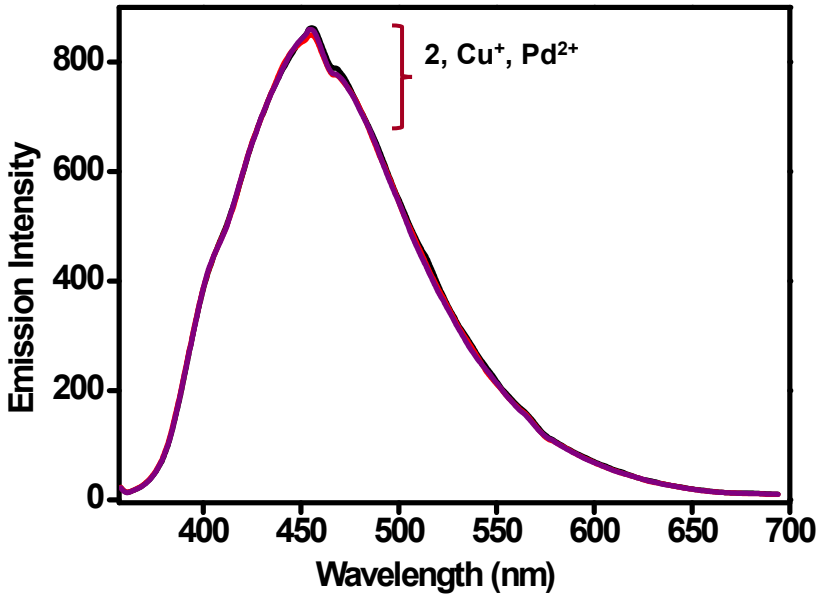

Figure S43. Emission spectra of MOF **2** in the presence of 50 μM of Cu^{+} and Pd^{2+} ions.

Table S1. Crystallographic data collection and structure refinement parameters for MOF **1**.

	1
Empirical formula	$C_{26}H_{23}N_3O_9SZn$
Formula weight	618.90
Temperature/K	273.15
Crystal system	monoclinic
Space group	*C*2/*c*
a/Å	34.862(4)
b/Å	9.8735(11)
c/Å	25.914(5)
α/°	90
β/°	130.261(2)
γ/°	90
Volume/Å^3	6806.6(16)
Z	8
ρ_{calc}g/cm^3	1.208
μ/mm^{-1}	0.829
F(000)	2544.0
Crystal size/mm^3	0.21 × 0.15 × 0.11
Radiation	MoKα (λ = 0.71073)
2Θ range for data collection/°	4.42 to 56.64
Index ranges	-46 ≤ h ≤ 46, -13 ≤ k ≤ 13, -34 ≤ l ≤ 34
Reflections collected	72085
Independent reflections	8471 [R_{int} = 0.0833, R_{sigma} = 0.0440]
Data/restraints/parameters	8471/0/367
Goodness-of-fit on F^2	1.055
Final *R* indexes [I>=2σ (I)]	R_1 = 0.0429, wR_2 = 0.1183
Final *R* indexes [all data]	R_1 = 0.0617, wR_2 = 0.1311
Largest diff. peak/hole / e Å^{-3}	0.62/-0.59
CCDC No.	2282501

Table S2. Selected bond distances (Å) for MOF **1**.

Bond	**1**
Zn(1)-O(4)$^{\#2}$	2.0432(18)
Zn(1)-O(5)$^{\#3}$	2.0408(18)
Zn(1)-O(7)$^{\#1}$	2.0354(19)
Zn(1)-O(6)	2.0296(18)

Symmetry transformations used to generate equivalent atoms: $^{\#1}$2-X,-Y,2-Z; $^{\#2}$+X,1-Y,1/2+Z; $^{\#3}$2-X,-1+Y,3/2-Z

Table S3. Selected bond angles (°) for MOF **1**.

Bond	1
O(4)$^{\#1}$-Zn(1)-Zn(1)$^{\#2}$	78.31(6)
O(5)$^{\#3}$-Zn(1)-Zn(1)$^{\#2}$	81.69(6)
O(5)$^{\#3}$-Zn(1)-O(4)$^{\#1}$	159.95(9)
O(7)$^{\#2}$-Zn(1)-Zn(1)$^{\#2}$	80.93a(6)
O(7)$^{\#2}$-Zn(1)-O(4)$^{\#1}$	90.00(8)
O(7)$^{\#2}$-Zn(1)-O(5)$^{\#3}$	88.28(8)
O(6)-Zn(1)-Zn(1)$^{\#2}$	78.76(6)
O(6)-Zn(1)-O(4)$^{\#1}$	85.24(8)
O(6)-Zn(1)-O(5)$^{\#3}$	89.47(8)
O(6)-Zn(1)-O(7)$^{\#2}$	159.68(9)
C(16)-O(4)-Zn(1)$^{\#4}$	129.20(18)
C(16)-O(5)-Zn(1)$^{\#5}$	124.54(17)
C(24)-O(7)-Zn(1)$^{\#2}$	125.70(18)
C(24)-O(6)-Zn(1)	129.02(19)

Symmetry transformations used to generate equivalent atoms: $^{\#1}$+X,1-Y,1/2+Z; $^{\#2}$2-X,-Y,2-Z; $^{\#3}$2-X,-1+Y,3/2-Z; $^{\#4}$+X,1-Y,-1/2+Z; $^{\#5}$2-X,1+Y,3/2-Z

Table S4. Fluorescence lifetime parameters for **1**, **1** + Pd^{2+} and **1** + Cu^{+}.

	T1 (ns)	**T2 (ns)**	**T3 (ns)**	**B1**	**B2**	**B3**	**Average Lifetime (ns)**
1	3.5023	1.9061	12.5051	0.02786	0.01351	0.0129	8.43
1 + Cu^{+}	3.1529	0.5258	14.5631	0.01801	0.12904	0.00274	4.84
1 + Pd^{2+}	3.1109	0.6843	16.1626	0.01757	0.11595	0.00253	5.06

Table S5. Crystallographic data collection and structure refinement parameters for MOF **2**.

	2
Empirical formula	$C_{28}H_{29}N_3O_9S_2Zn$
Formula weight	681.03
Temperature/K	100.15
Crystal system	monoclinic
Space group	*P*2/*n*
a/Å	18.1952(6)
b/Å	8.3525(2)
c/Å	21.6671(6)
α/°	90
β/°	94.039(3)
γ/°	90
Volume/Å^3	3284.69(16)
Z	4
ρ_{calc}g/cm^3	1.377
μ/mm^{-1}	0.927
F(000)	1408.0
Crystal size/mm^3	0.20 × 0.16 × 0.12

Radiation	MoKα (λ = 0.71073)
2Θ range for data collection/°	6.23 to 62.04
Index ranges	-25 ≤ h ≤ 19, -9 ≤ k ≤ 11, -31 ≤ l ≤ 29
Reflections collected	38109
Independent reflections	8794 [R_{int} = 0.0468, R_{sigma} = 0.0427]
Data/restraints/parameters	8794/0/398
Goodness-of-fit on F^2	1.038
Final R indexes [I>=2σ (I)]	R_1 = 0.0727, wR_2 = 0.2022
Final R indexes [all data]	R_1 = 0.1002, wR_2 = 0.2230
Largest diff. peak/hole / e Å^{-3}	0.36/-1.36
CCDC No.	2282500

Table S6. Selected bond distances (Å) for MOF **2**.

Bond	2
Zn(1)-O(6)	1.946(3)
Zn(1)-O(7)$^{\#1}$	1.958(3)
Zn(1)-O(8)	1.972(3)
Zn(1)-O(5)$^{\#2}$	1.939(3)

Symmetry transformations used to generate equivalent atoms: $^{\#1}$-X,1-Y,1-Z; $^{\#2}$-1/2+X,-Y,-1/2+Z

Table S7. Selected bond angles (°) for MOF **2**.

Bond	2
O(6)-Zn(1)-O(7)$^{\#1}$	116.74(12)
O(6)-Zn(1)-O(8)	103.35(12)
O(7)$^{\#1}$-Zn(1)-O(8)	96.10(12)
O(5)$^{\#2}$-Zn(1)-O(6)	115.79(13)
O(5)$^{\#2}$-Zn(1)-O(7)$^{\#1}$	104.54(13)
O(5)$^{\#2}$-Zn(1)-O(8)	119.24(13)
C(24)-O(6)-Zn(1)	135.5(3)
C(24)-O(7)-Zn(1)$^{\#1}$	121.5(3)
S(1)-O(8)-Zn(1)	121.92(16)
C(16)-O(5)-Zn(1)$^{\#3}$	108.8(3)

Symmetry transformations used to generate equivalent atoms: $^{\#1}$-X,1-Y,1-Z; $^{\#2}$-1/2+X,-Y,-1/2+Z; $^{\#3}$1/2+X,-Y,1/2+Z